Article

Cell Chemical Biology

# Non-canonical function of histone methyltransferase G9a in the translational regulation of chronic inflammation

## Graphical abstract

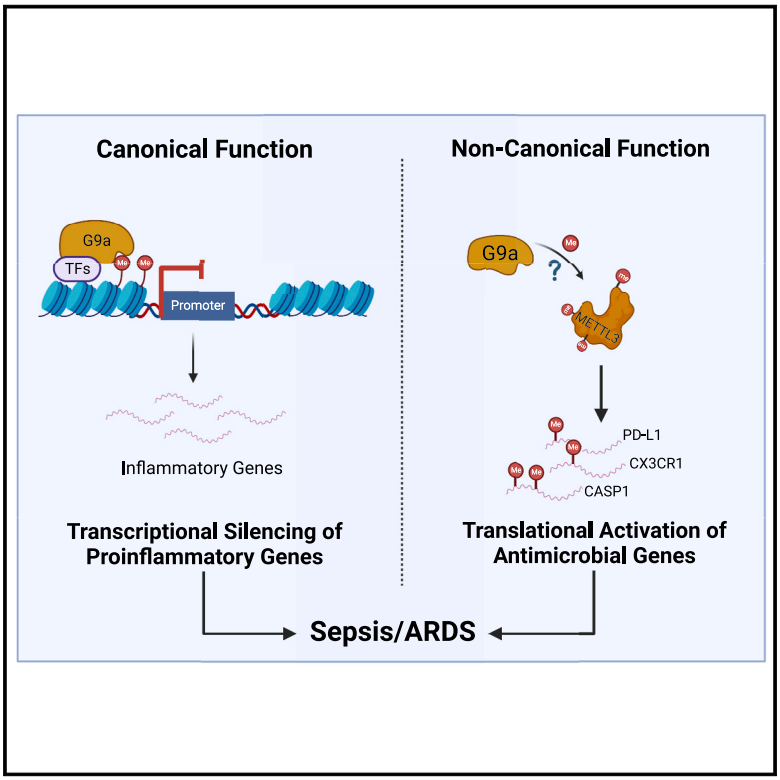


## Authors

Adil Muneer, Li Wang, Ling Xie, ..., Hongjun Song, Jian Jin, Xian Chen

## Correspondence

xianc@email.unc.edu

## In brief

Muneer et al. reveal that G9a—a histone methyltransferase and well-established transcriptional repressor—promotes macrophage proliferation, T cell depletion/dysfunction (lymphopenia), and organ-damaging "cytokine storm" (hyperinflammation) through its non-canonical/non-epigenetic function involving protein translation, a mechanism that can be leveraged to treat chronic inflammatory diseases including sepsis, ARDS, & COVID19.

## Highlights

- G9a interacts with distinct translation regulators to modulate protein translation
- G9a-METTL3-m$^6$A axis promotes hyper-inflammation and T cell dysfunction
- G9a promotes turnover of chronic disease-related proteins in ET macrophages
- G9a inhibition hinders proteostasis of chronic disease-related proteins

Muneer et al., 2023, Cell Chemical Biology *30*, 1–17
December 21, 2023 © 2023 Elsevier Ltd.
https://doi.org/10.1016/j.chembiol.2023.09.012

CellPress

Please cite this article in press as: Muneer et al., Non-canonical function of histone methyltransferase G9a in the translational regulation of chronic inflammation, Cell Chemical Biology (2023), https://doi.org/10.1016/j.chembiol.2023.09.012

Cell Chemical Biology

CellPress

Article

# Non-canonical function of histone methyltransferase G9a in the translational regulation of chronic inflammation

Adil Muneer,[1,8] Li Wang,[1,8] Ling Xie,[1,8] Feng Zhang,[5] Bing Wu,[3] Liu Mei,[1] Erik M. Lenarcic,[3] Emerald Hillary Feng,[1] Juan Song,[4] Yan Xiong,[6] Xufen Yu,[6] Charles Wang,[7] Kanishk Jain,[1,2] Brian D. Strahl,[1,2] Jeanette Gowen Cook,[1,2,4] Yisong Y. Wan,[3] Nathaniel John Moorman,[3] Hongjun Song,[5] Jian Jin,[6] and Xian Chen[1,2,9,*]

[1]Department of Biochemistry & Biophysics, University of North Carolina at Chapel Hill, Chapel Hill, NC 27599, USA
[2]Lineberger Comprehensive Cancer Center, University of North Carolina at Chapel Hill, Chapel Hill, NC 27599, USA
[3]Department of Microbiology and Immunology, University of North Carolina at Chapel Hill, Chapel Hill, NC 27599, USA
[4]Department of Pharmacology, University of North Carolina at Chapel Hill, Chapel Hill, NC 27599, USA
[5]Department of Neuroscience and Mahoney Institute for Neurosciences, University of Pennsylvania, Philadelphia, PA 19104, USA
[6]Mount Sinai Center for Therapeutics Discovery, Departments of Pharmacological Sciences and Oncological Sciences, Tisch Cancer Institute, Icahn School of Medicine at Mount Sinai, New York, NY 10029, USA
[7]Center for Genomics, Division of Microbiology & Molecular Genetics, Department of Basic Sciences, Loma Linda University, Loma Linda, CA 92350, USA
[8]These authors contributed equally
[9]Lead contact
*Correspondence: xianc@email.unc.edu
https://doi.org/10.1016/j.chembiol.2023.09.012

## SUMMARY

We report a novel translation-regulatory function of G9a, a histone methyltransferase and well-understood transcriptional repressor, in promoting hyperinflammation and lymphopenia; two hallmarks of endotoxin tolerance (ET)-associated chronic inflammatory complications. Using multiple approaches, we demonstrate that G9a interacts with multiple translation regulators during ET, particularly the N6-methyladenosine ($m^6A$) RNA methyltransferase METTL3, to co-upregulate expression of certain $m^6A$-modified mRNAs that encode immune-checkpoint and anti-inflammatory proteins. Mechanistically, G9a promotes $m^6A$ methyltransferase activity of METTL3 at translational/post-translational level by regulating its expression, its methylation, and its cytosolic localization during ET. Additionally, from a broader view extended from the G9a-METTL3-$m^6A$ translation regulatory axis, our translatome proteomics approach identified numerous "G9a-translated" proteins that unite the networks associated with inflammation dysregulation, T cell dysfunction, and systemic cytokine response. In sum, we identified a previously unrecognized function of G9a in protein-specific translation that can be leveraged to treat ET-related chronic inflammatory diseases.

## INTRODUCTION

Inflammation is a key host innate immune response to microbial and pathogen challenge. Ordinarily, the immune system releases inflammatory factors to combat an infection. However, by largely unknown mechanisms, dysregulated inflammation can result in severe immunopathogenic consequences such as sepsis and acute respiratory distress syndrome (ARDS). For example, sepsis is a dysregulated inflammatory response elicited by gram-negative bacterial infection[1,2] and is the third leading cause of death in the US after heart disease and cancer.[3,4] Sepsis occurs when immunity is unbalanced so that harmful anti-inflammatory factors are released in a "cytokine storm" that damages multiple organs.[5] Sepsis has no cure because a lack of detailed mechanistic understanding of its pathogenesis has severely restrained effective therapeutic options.

Endotoxin (lipopolysaccharide, LPS) tolerance (ET)[6,7] is a principal feature of many chronic inflammatory diseases and associated complications including sepsis and ARDS. Primary molecular characteristics of ET-related sepsis include (1) down-regulation of "tolerizeable" pro-inflammatory mediators, such as TNF-$\alpha$, IL-1$\beta$, and CXCL10, and (2) upregulation of "non-tolerizeable" anti-microbial or anti-inflammatory cytokines such as IL-10 and TGF-$\beta$. These inflammatory characteristics together contribute to impaired adaptive immunity (e.g., T cell exhaustion or a poor switch to the adaptive response) and susceptibility to secondary infection with an organ-damaging cytokine storm.[6] The current model of inflammation control in ET macrophages, derived primarily from RNA expression studies,[8,9] involves gene-specific reprogramming of chromatin and associated histone modifications. That is, with prolonged LPS stimulation, chromatin of pro-inflammatory (tolerizeable)

Please cite this article in press as: Muneer et al., Non-canonical function of histone methyltransferase G9a in the translational regulation of chronic inflammation, Cell Chemical Biology (2023), https://doi.org/10.1016/j.chembiol.2023.09.012



genes transitions from transcriptionally active to a transcriptionally silent state while the other class of anti-microbial (non-tolerizeable) genes remains transcriptionally active in ET.[10,11] Epidemiology showed that the activity of the histone methyltransferases G9a (EHMT2) and G9a-like protein (GLP; hereafter G9a will represent both proteins) was induced in sepsis patients with trauma.[12] Accordingly, we showed that G9a suppressed the transcription of certain pro-inflammatory genes in ET via interactions with transcription factors such as cMyc.[13] However, this canonical, transcription-silencing function of G9a did not explain how translation of mRNAs encoding anti-microbial or anti-inflammatory proteins was upregulated in the immunocompromised ET macrophage cells in which G9a is constitutively (enzymatically) active.

We reported that inhibition of G9a activity mitigated or reversed ET,[13] thereby linking G9a activity to the ET phenotype. Thus, we first employed our chromatin activity-based chemoproteomics (ChaC)-mass spectrometry (MS) approach using UNC0965,[14] a biotin-conjugated small molecule inhibitor of G9a/GLP, as a mechanistic probe[15] to dissect G9a/GLP-associated pathways and mechanisms in ET. ChaC has unique strengths to discover new functions of constitutively active G9a, which can be extrapolated by identifying active G9a interactors with known functions[16,17] As expected, ChaC-MS captured certain transcriptional regulatory proteins. Unexpectedly, however, quantitative ChaC-MS also identified numerous G9a-interacting proteins that are functionally associated with translation initiation/elongation, RNA metabolism and processing, ribosomal biogenesis, and protein degradation. Specifically, we detected increased interaction between G9a and several regulators of N6-methyladenosine ($m^6A$) modification that function during ET. A notable G9a interactor was METTL3, an RNA methyltransferase that catalyzes $m^6A$ modification of RNA to promote oncogene translation[18] and is implicated in inflammation.[19–21] Additionally, in the same ET-characteristic UNC0965 pull-down complex,[22] G9a had enhanced interaction with members of NOP56p-associated pre-ribosomal(r)RNA complex, including FBL that directs rRNA 2′-*O*-methylation[23] and enhancer of zeste homolog 2 (Ezh2). Based on our quantitative ChaC-MS identification of METTL3, Ezh2, FBL, and other G9a activity-dependent translation regulators, we hypothesized that, via interactions with these regulators of translation or ribosome biogenesis, constitutively active G9a has a non-canonical (non-epigenetic) function in regulating translation-related pathways or mechanisms in ET.

As the first step to test the aforementioned hypothesis, i.e., G9a activity may broadly impact translation to promote ET, we investigated whether and how G9a activity regulates METTL3/$m^6A$-mediated translation in ET. We used approaches that included $m^6A$ RNA immunoprecipitation-seq (RIP-seq), label-free quantitative proteomics,[24–26] tandem mass spectrometry (MS/MS) peptide sequencing, and molecular/cellular biology and immunological assays. We found that G9a upregulates $m^6A$ methyltransferase activity of METTL at the translational and post-translational modification (methylation) level. Specifically, G9a activity regulates ET-characteristic expression, subcellular localization, and methylation of METTL3 to promote expression of proteins involved in survival/proliferation of inflammatory cytokine-producing macrophage cells[27] and impairment of T cell function,[28] two hallmarks of ET-associated diseases such as sepsis and ARDS.

Further, we employed a quantitative translatome proteomic approach to identify proteins on a genomic scale that showed G9a-dependent translation (G9a-translated proteins) in ET macrophages. In correlation with numerous ChaC-identified interactors that were reported as putative nonhistone substrates of G9a/GLP, translatome analysis validated the global impact of G9a translational mechanism: From a broader view extended from the G9a-METTL3-$m^6A$ translation regulatory axis, G9a activates the widespread translation of broad-spectrum proteins that unite the networks associated with sepsis and ARDS, particularly the sepsis-characteristic overexpression of an immune checkpoint protein CD274 (programmed cell death-ligand 1 or PD-L1).[28] Correspondingly, inhibition of G9a or its interactor Ezh2 similarly reduced expression of select G9a-translated proteins, which confirmed the function of the G9a interactome in the ET-characteristic translational regulation.

Overall, we showed that, in parallel with G9a-mediated transcriptional repression of ‘‘tolerizeable’’ pro-inflammatory genes for immunosuppression, G9a is non-canonically committed to the translational activation of ‘‘non-tolerizeable’’ or anti-microbial proteins in ET. To our knowledge, this involvement of G9a is the first reported instance of a unifying molecular mechanism that accounts for both immunosuppressive and anti-microbial phenotypes of ET. Correspondingly, the G9a-METTL3-$m^6A$ axis was shown to account for only a subset of G9a-translated proteins in ET, which suggested that, via interactions with multiple translation regulators other than METTL3, such as Ezh2, G9a coordinates additional, yet to be characterized mechanisms to facilitate protein-specific translation. Thus, further study is warranted regarding G9a’s function in global protein translation or turnover. More importantly, we show that this newly discovered G9a-mediated translational phenomenon can be leveraged to hinder proteostasis (i.e., expression, secretion, and/or turnover) of chronic inflammatory disease-related factors in sepsis and ARDS, which represents an attractive target for therapeutic intervention.

## RESULTS

### Constitutively active G9a is implicated in translational regulation of ET

Previously, we found by top-down mass spectrometry (MS), ChIP-PCR, and ChaC analysis that the methylation activity of G9a was constitutively higher in chronically inflamed (TL) or endotoxin-tolerant (ET) macrophages compared with acutely inflamed (NL) cells.[13] Accordingly, to dissect G9a-interacting pathways in ET, we first performed label-free quantitation (LFQ)[25,26] based ChaC-MS experiments using UNC0965, a biotinylated inhibitor of G9a/GLP,[15] in murine macrophage cells (Raw 264.7) under non-stimulated (N), acutely inflamed, and chronically inflamed (TL)/ET conditions (Figures 1A and S1A). On the basis of LFQ ratios that are proportional to relative binding of individual proteins to G9a in TL(ET) versus N or NL, we identified 365 proteins that showed consistently enhanced interaction with G9a in TL macrophages (Figures S1B and S1C; Table S1A). In agreement with G9a’s canonical transcription regulatory function, several of these ET-specific G9a interactors were associated

Please cite this article in press as: Muneer et al., Non-canonical function of histone methyltransferase G9a in the translational regulation of chronic inflammation, Cell Chemical Biology (2023), https://doi.org/10.1016/j.chembiol.2023.09.012



CellPress

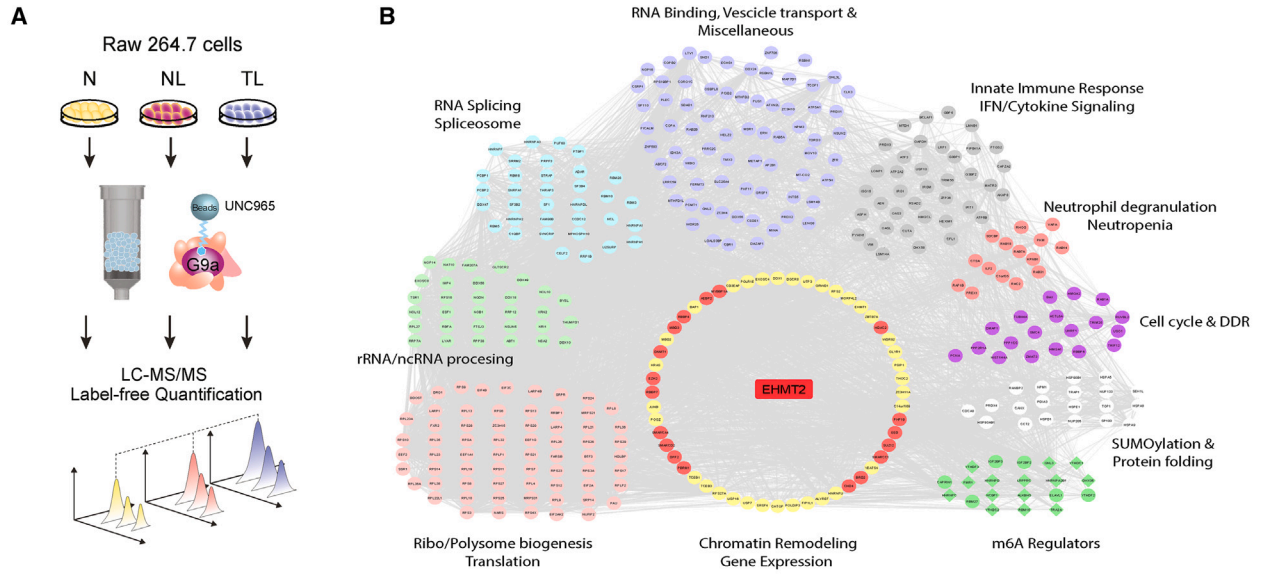


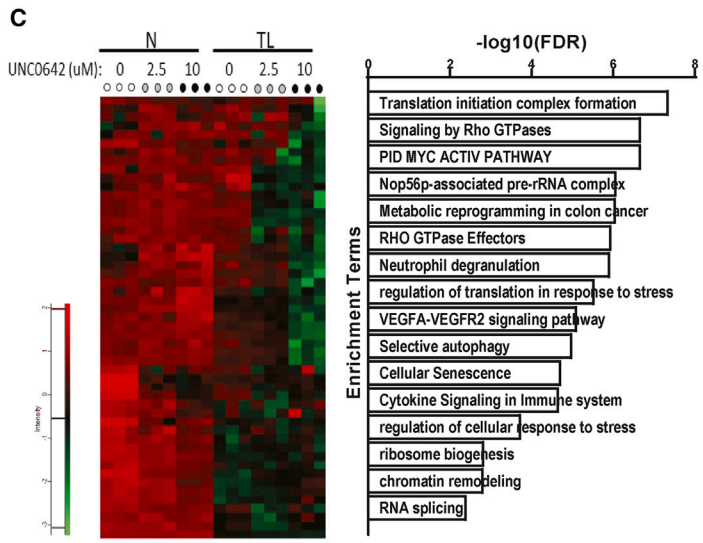


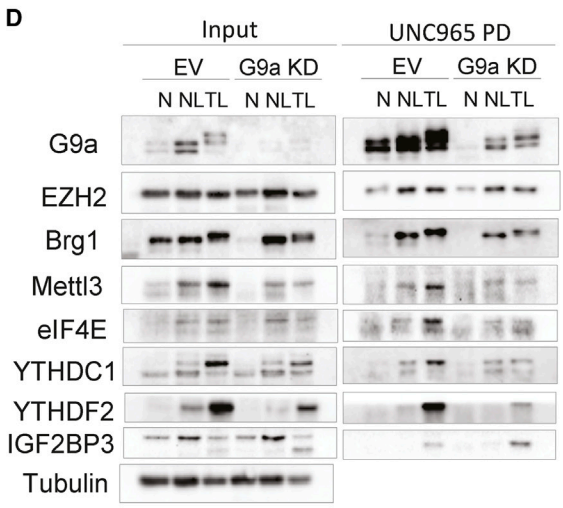


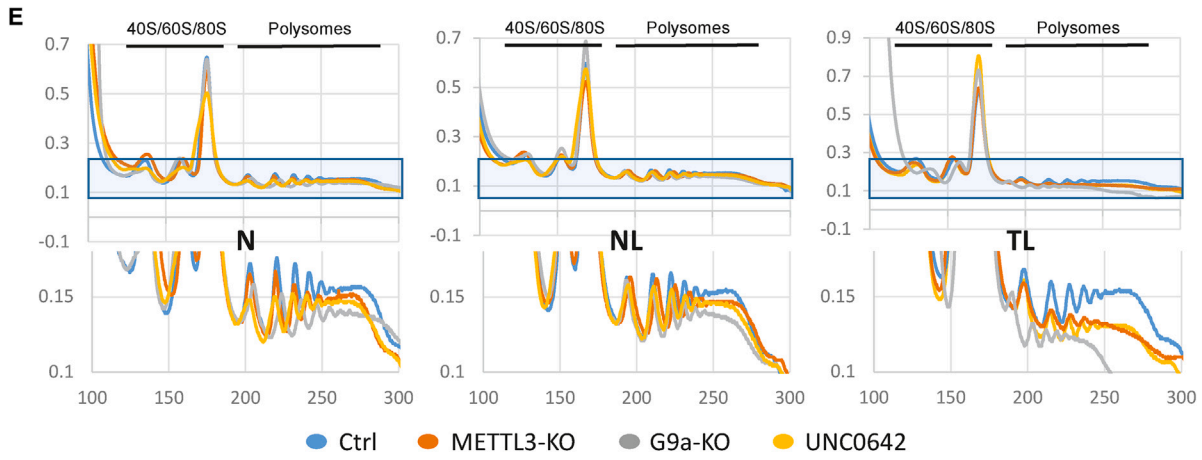


*(legend on next page)*

Please cite this article in press as: Muneer et al., Non-canonical function of histone methyltransferase G9a in the translational regulation of chronic inflammation, Cell Chemical Biology (2023), https://doi.org/10.1016/j.chembiol.2023.09.012



with chromatin remodeling and gene expression, such as the PRC2 complex, the SWI/SNF complex, and BRD4. In addition, ChaC LFQ-MS identified enhanced associations of G9a with numerous translation-associated proteins that function in e.g., m$^6$A modification, rRNA/ribosome/polysome biogenesis, RNA processing, immunity, and SUMOylation/protein-folding (Figure 1B).

We next validated dependence of these translation-related interactions on the enzymatic activity of G9a by performing inhibitor competition ChaC experiments in Raw264.7 macrophage cells under N and TL conditions. As a UNC0965 competitor, we used 99.95% pure UNC0642 (a non-tagged inhibitor of G9a) that potently binds to active G9a at IC50 < 2.5 nM.[29] Increasing amounts of UNC0642 progressively displaced constitutively active G9a binding to UNC0965 (Figure S1D). In parallel, LFQ ChaC-MS identified 174 proteins whose binding to UNC0965 was reduced following UNC0642 pre-treatment (Table S1B). As expected, the majority of these G9a activity-dependent interactors are functionally associated with translation regulation, rRNA/ribosome biogenesis, immunity, and RNA splicing (Figure 1C). These results validated the specificity of binding between these translation regulators and constitutively active G9a, which is the determinant of G9a function in the translational regulation.

G9a and GLP lay down H3K9-me1/2 marks by way of their catalytic SET domain, and they bind the same marks (methylated lysine; Kme) by way of their ankyrin repeat regions. In agreement with these facts, many ET-specific G9a interactors (Figure 1B) that were verified by competition quantitative ChaC-MS (Figure 1C) are known or putative nonhistone substrates of G9a, mostly involved in ribosome biogenesis (Figure S1E). Altogether, combined ChaC-MS results suggest that, via interaction and/or methylation of various translation regulators, G9a coordinates ET-promoting translation in a SET domain-dependent manner.

## G9a and METTL3 coregulate m$^6$A-mediated translation of pro-ET proteins

Notably, among the ChaC-identified G9a interactors, a cluster of m$^6$A readers and writers showed increased interaction with G9a in ET macrophages (Figure 1B). Reciprocal IP-MS experiments using Flag-tagged METTL3, the methyltransferase responsible for m$^6$A modification, also detected G9a complex members (EHMT1, EHMT2, WIZ) along with most of the ET-specific translation regulatory proteins identified by ChaC-MS (Figure S1F; Table S1C). These results from unbiased interactome screening indicated that G9a and METTL3 function in the same translation regulatory pathways. In agreement with the ChaC and IP-MS results, immunoblotting further confirmed ET/TL-specific association of endogenous G9a with various m$^6$A writers (METTL3) and readers (YTHDC1, YTHDF2, IGF2BP3, HNRNPA2B1) along with other translation regulators including eIF4E. In macrophage cells with G9a knock-down, UNC0965 pulled down only proteins that interacted with residual G9a (Figures 1D and S1G). Pre-treatment with excess UNC0642 reduced the amount of METTL3 in UNC0965 pull-downs, further confirming specificity of G9a-METTL3 interaction during ET (Figure S1G). These results, coupled with the fact that METTL3 promotes mRNA translation in both methyltransferase activity-dependent and independent manner,[18] led us to investigate the function of G9a in m$^6$A/METTL3-regulated translation during ET.

We used CRISPR/Cas9 to knock out (KO) G9a or METTL3 in macrophages subjected to LPS stimulation to generate cells with different inflammatory conditions (NL, T, or TL). As indicated by reduced levels of proinflammatory markers such as phospho-p65 and phospho-IkB in macrophages under prolonged LPS stimulation, depletion of either METTL3 or G9a caused reduced ET and re-sensitized ET macrophages to LPS stimulation (Figures S1H and S1I). These results suggested that ET is coregulated by G9a and METTL3. Next, we measured global protein synthesis based on polysome abundance in wild type versus G9a KO and METTL3 KO macrophages.[30] Polysome abundance similarly decreased in G9a KO, G9a inhibitor (UNC0642) treated, and METTL3 KO cells compared with wild-type controls under LPS-treated and untreated conditions (Figure 1E). Thus, depletion of either G9a or METTL3 suppressed global protein synthesis in murine macrophage cells. Further, because cytosolic translocation of METTL3 is correlated with its translation activity,[18] we investigated the effect of G9a activity/expression on the subcellular distribution of METTL3 under non-stimulated (N) and endotoxin tolerant (TL/ET) conditions. Coincident with the ET-promoting function of METTL3, more METTL3 was present in the cytosol of TL macrophages compared with unstimulated controls, and genetic depletion or pharmacologic inhibition of G9a reduced cytosolic METTL3 (Figure S1J). In sum, G9a interacts with METTL3 and regulates its expression and subcellular localization in ET macrophages to potentially regulate METTL3/m$^6$A-dependent translation.

To further clarify how G9a/METTL3-coregulated translation determines the ET phenotype, we sought to identify specific mRNAs whose translation was dependent on G9a and

**Figure 1. Constitutively active G9a is involved in translational regulatory pathways in ET**

(A) Schematic of ChaC-MS based dissection of G9a interactome in murine macrophage cells (Raw264.7) under different inflammatory conditions (N, NL, TL).

(B) Network depicting overrepresented terms among ChaC-identified G9a interactors in chronically inflamed macrophages (TL/ET), compared to cells under N or NL. Physical interactions were curated from StringDB.

(C) Heatmap of ET/TL-specific G9a interactors in Raw264.7 macrophage cells (left), identified and enriched by UNC0965-based ChaC-MS (FC > |1.4|; p < 0.05) following UNC0642 pre-treatment (n = 3) at indicated concentrations. Specific interactors were competed off by UNC0642 pre-treatment, compared with DMSO-treated controls. Enrichment analysis for indicated proteins is included (right).

(D) Immunoblots showing increased association between endogenous G9a and various m$^6$A regulators in TL compared with N or NL, with Ezh2 and Brg1 included as positive controls. The Raw264.7 macrophage cell lines either stably expressing shRNA for G9a knockdown (KD) or empty vector (EV) for G9a wild type. Left = inputs and right = UNC0965 pull-down (PD). Some interactors were pulled down from G9a KD cells because of residual G9a.

(E) Polysome analysis of G9a- or METTL3-dependent protein synthesis in Raw264.7 cells. Absorbance profiles of sucrose density gradients show the location of 40S and 60S ribosomal subunits, 80S monosomes, and polysomes (top). Zoom-in area focuses on polysomes (bottom). Results shown are from biological duplicate.

See also Figure S1 & Table S1.

Please cite this article in press as: Muneer et al., Non-canonical function of histone methyltransferase G9a in the translational regulation of chronic inflammation, Cell Chemical Biology (2023), https://doi.org/10.1016/j.chembiol.2023.09.012



CellPress

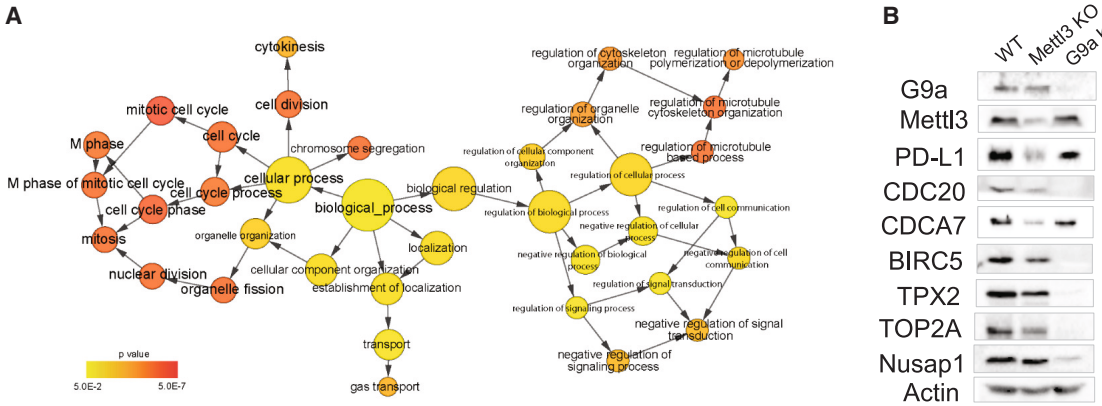


*(legend on next page)*

Please cite this article in press as: Muneer et al., Non-canonical function of histone methyltransferase G9a in the translational regulation of chronic inflammation, Cell Chemical Biology (2023), https://doi.org/10.1016/j.chembiol.2023.09.012



METTL3. Accordingly, we performed RNA-seq and m$^6$A RNA immunoprecipitation-sequencing (MeRIP-Seq) on wild type, G9a KO, and METTL3 KO human macrophage cells (THP1) under different inflammatory conditions (N, NL, TL). First, in the G9a-depleted macrophages under TL, 440 immune or inflammatory response genes exhibited increased mRNA abundance (Figure S2A; Table S2A). This finding of G9a-suppressed genes aligned with our previous report[13] that, via interactions with transcriptional repressors such as cMyc, constitutively active G9a suppresses the transcription of proinflammatory genes. Conversely, we identified, in both G9a KO and METTL3 KO cells under TL, 136 genes with decreased mRNA expression compared to wild-type cells (Table S2A); these genes were associated mostly with regulation of cell cycle progression, cell proliferation, and anti-viral or anti-inflammatory responses (Figure 2A). Like the co-existence of G9a and METTL3 in TL-specific translation regulatory complexes, this new finding of G9a/METTL3-co-upregulated genes indicated that G9a and METTL3 cooperate to post-transcriptionally activate expression of pro-survival and anti-inflammatory proteins in TL. Further, 62 of 136 G9a/METTL3-co-upregulated genes were tagged with m$^6$A (Figure 2A). The integrative genomics viewer plots showed that the m$^6$A level of most mRNAs that encode these G9a/METTL3-co-upregulated proteins decreased in either G9a KO or METTL3 KO macrophages with TL (Figure S2B). Notably, the ''stabilized'' or ''actively translated'' mRNA (total input) that was proportional to the amount of m$^6$A-tagged transcripts also showed a dependence on both G9a and METTL3. We also validated by quantitative PCR the G9a- and METTL3-dependence of the abundance of m$^6$A-tagged mRNA coding these proteins (Figure S2C).

Next, we performed LFQ proteomics to identify proteins that exhibited G9a- or METTL3-dependent expression changes in the same THP-1 macrophage set (e.g., wild type versus G9a KO versus METTL3) (Table S2B). Principal component analysis (Figure S2D) showed that, in TL, G9a KO or METTL3 KO produced clusters of protein expression profiles that were well separated from the clusters of wild type macrophages in ET. This result indicated that depletion of G9a and METTL3 led to characteristic protein expression patterns that represented similar inflammatory phenotypes. To determine which proteins were coregulated by G9a and METTL3 at the translational level, we compared the m$^6$A transcriptome and proteome data of the same sample sets including wild type versus G9a KO versus METTL3 KO (Table S2B). The G9a/METTL3-co-upregulated m$^6$A mRNA or their encoded proteins that we identified by nonbiased MeRIP-seq or LFQ proteomics functionally overlapped with the pathways related to antiviral immune response and cell fate determination (Figure S2E). Immunoblotting confirmed that expression of proteins in these functional clusters had a dual dependence on G9a and METTL3 (Figure 2B), which indicated that G9a and METTL3 coactivate translation of the same sets of m$^6$A-tagged mRNA. In agreement with our ChaC-MS finding of enhanced interactions of G9a with METTL3 and associated translational regulatory proteins (Figure 1B), this m$^6$A epitranscriptomic-to-proteomic correlation for specific proteins indicated that, via interaction with METTL3 complex, G9a and METTL3 work in concert in the same translation regulatory pathways that define the ET phenotype.

## G9a and METTL3 promote proliferation of ET macrophages that produce hyperinflammatory factors

One cluster of proteins co-upregulated by G9a and METTL3 was composed of BIRC5,[31] CDC20,[32,33] NUSAP1,[34] CDCA7,[35] TOP2A, and ALCAM, functionally associated with cell division, mitotic cell cycle, and cell proliferation[34,36–39] (Figure 2A). This observation not only aligned with the function of METTL3 in promoting cell cycle progression and survival,[40] but more importantly implicated constitutively active G9a in promoting METTL3-mediated translation of pro-survival proteins, e.g., METTL3-mediated m$^6$A promotes translation of cMyc mRNA and is responsible for cMyc stability in AML cells.[41] Therefore, we used flow cytometry to determine the effect of G9a and METTL3 on the cell cycle in different inflammatory conditions. Conditions that mimicked chronic inflammation (TL/ET) caused a dramatic accumulation of macrophages in G1 compared with non-stimulated (N) or acutely inflamed (NL) conditions (72% vs. 46%; Figure 2C). This G1 accumulation was accompanied by fewer S phase cells (23% vs. 43%). Neither G9a nor METTL3 knockout delayed the G1 phase under the TL condition. Prolonged LPS stimulation (TL) caused these G9a- or METTL3-knockout lines to spend more time in S phase relative to wild-type cells and relative to the same cells under acute inflammation conditions. The clonogenic assay (Figure 2D) showed both knockout lines survived less well than controls during TL treatment, and the G1 delay could serve a protective function. Akin to our proteomic finding that G9a and METTL3 coactivate expression of multiple pro-survival proteins, these cell cycle analyses indicated that constitutively active G9a and METTL3 cooperate to restrain cell cycle progression and promote increased survival of the slow-processing macrophages during

**Figure 2. G9a and METTL3 cooperate to dysregulate cell cycle and impair T cell function under ET**

(A) Overrepresented terms for 136 mRNAs co-downregulated following G9a KO and METTL3 KO in THP-1 cells under TL (RNA-Seq; $p < 0.05$).

(B) Immunoblot of protein expression in wild-type versus G9a KO or METTL3 KO THP-1 cells under TL.

(C) LPS-induced cell-cycle arrest in endotoxin-tolerant conditions requires G9A and METTL3. Flow cytometry of the impact of G9a and METTL3 on cell cycle in different inflammatory conditions (e.g., N, NL, or TL). Cells were labeled with EdU (10 $\mu$ M) for 30 min before harvesting and analyzed by flow cytometry for DNA content with DAPI and for DNA synthesis with EdU.

(D) Clonogenic survival assay of WT and KO Raw 264.7 cells in different inflammation conditions. WT cells were either treated with DMSO (0.05%) or 1 mM G9a inhibitor (UNC0642) or 1 mM EZH2 inhibitor (UNC1999). Mean ± SD of three independent experiments. *$p < 0.05$, **$p < 0.01$ versus control cells.

(E) Depletion of METTL3 or G9a promotes T cell activation and proliferation under the TL conditions. Histograms obtained from the CD8 T cell activation (upper panel) and proliferation (lower panel). The proliferation and activation markers, including CD25 of P14 CD8$^+$ T cells, were analyzed by flow cytometry at day 5 and day 6 after coculture with wild-type, METTL3 knock-out (KO) or G9a KO RAW 264.7 cells that were untreated (N) or treated with an acute LPS stimulation (NL) and prolonged LPS stimulation (TL), a mimic of ET.

See also Figure S2; Table S2.

Please cite this article in press as: Muneer et al., Non-canonical function of histone methyltransferase G9a in the translational regulation of chronic inflammation, Cell Chemical Biology (2023), https://doi.org/10.1016/j.chembiol.2023.09.012



CellPress

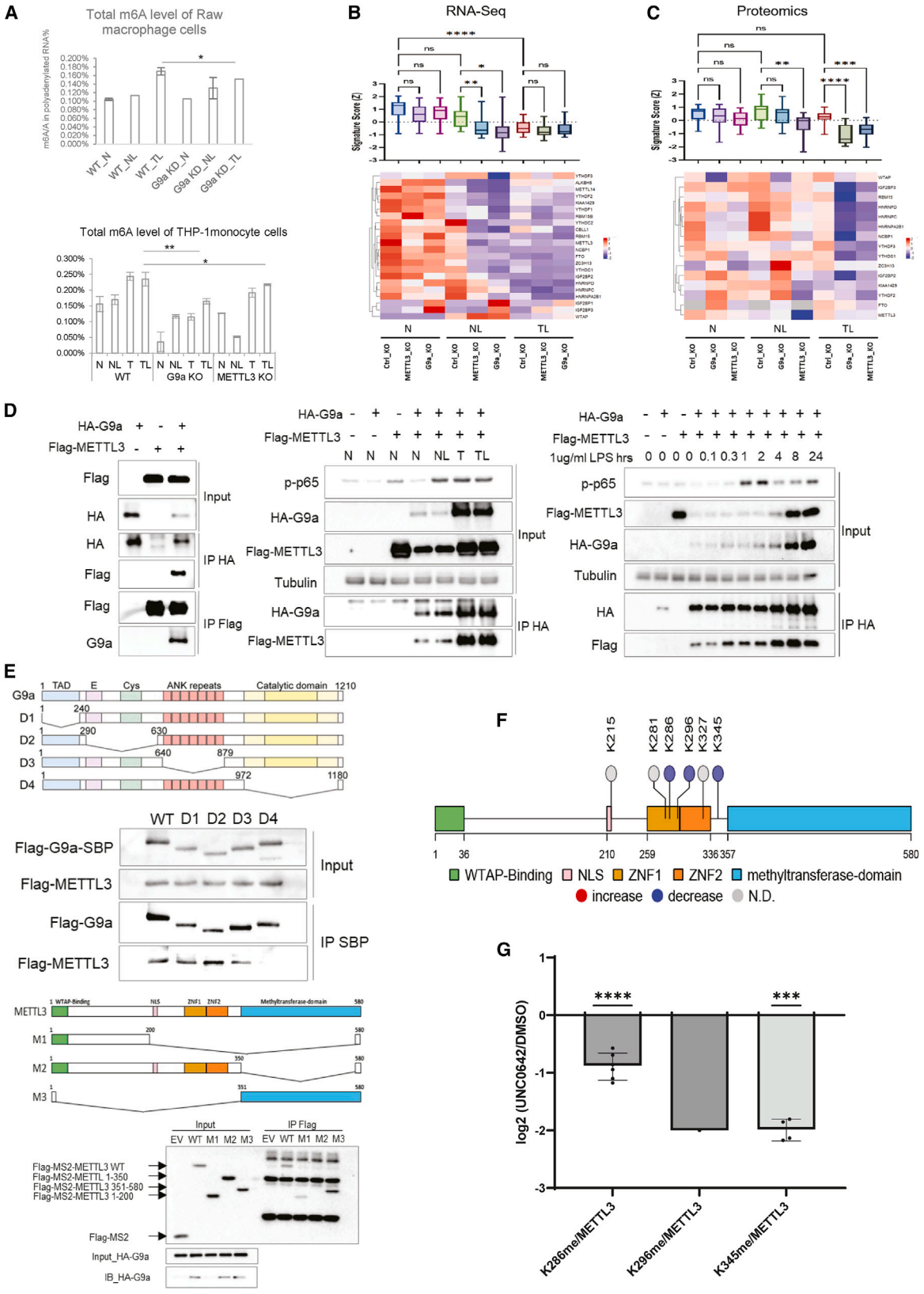


*(legend on next page)*

Please cite this article in press as: Muneer et al., Non-canonical function of histone methyltransferase G9a in the translational regulation of chronic inflammation, Cell Chemical Biology (2023), https://doi.org/10.1016/j.chembiol.2023.09.012



chronic inflammation, possibly by targeting pro-survival mRNAs for translation specifically in the growth phase (G1).

## G9a and METTL3 co-upregulated ET overexpression of PD-L1 to impair T cell function

Another cluster of G9a/METTL3-co-upregulated proteins composed of PD-L1, CX3CR1, and IRF8 is functionally associated with immune checkpoint regulation and antimicrobial response. PD-L1 is overexpressed in sepsis with impaired T cell function[28]; likewise, our MeRIP-seq data showed an increased level of PD-L1 (CD274) m$^6$A mRNA under ET (Figure S2B). Although PD-L1 m$^6$A mRNA exhibited little dependence on G9a or METTL3 similar to certain METTL3-regulated genes,[18] results from LFQ proteomics and immunoblotting consistently showed that the ET overexpression of PD-L1 was dependent on G9a and METTL3 (Figures 2B and S2E). Thus, we hypothesized that G9a and METTL3 impair T cell function via promoting translation or overexpression of PD-L1 in ET macrophages. To test this hypothesis, we performed a similar T cell proliferation assay[42] to determine the effect of either G9a KO or METTL3 KO on T cell function under the TL/ET condition. We compared T cell activation and proliferation by incubation of wild type, G9a KO, or METTL3 KO Raw cells collected under different inflammatory conditions (N, NL, and TL) with T cells from a P14 transgenic mouse. By monitoring T cell activation marker CD25, we observed that the co-existing TL/ET wild-type cells suppressed activation of CD8$^+$ T cells, whereas incubation with G9a KO or METTL3 KO cells produced efficiently activated T cells (Figure 2E, upper panel). Similarly, we found a greater number of proliferated P14 CD8$^+$ T cells after six days of co-incubation of T cells with either G9a KO or METTL3 KO cells, whereas wild-type cells lost the ability to promote proliferation of T cells in ET (Figure 2E, lower panel). Overall, these results showed that G9a and METTL3 impair T cell function by promoting overexpression of immune checkpoint proteins such as PD-L1.

## G9a regulates METTL3-driven translation at the translational and post-translational levels

To investigate how G9a regulates METTL3-dependent translation, we first looked at the total m$^6$A level of RNA under different inflammatory conditions (N, NL, T, and TL). Prolonged endotoxin treatment (T/TL) increased global m$^6$A modification in Raw 264.7 and THP-1 macrophages compared with unstimulated controls (N), whereas G9a KO and METTL3 KO reduced m$^6$A levels across all inflammatory conditions (Figure 3A). Interestingly, despite no change in transcript levels (Figure 3B), protein expression of METTL3 decreased significantly following G9a KD in ET macrophages (Figures 1D and S1G), where both G9a and METTL3 were induced. However, UNC0642 treatment did not affect METTL3 expression (Figure S1G) but altered its subcellular localization (Figure S1J) in ET macrophages. These findings suggested that G9a regulates METTL3 expression and/or methyltransferase activity at the post-translational level. In contrast, protein expression of other m$^6$A regulators remained largely unchanged in ctrl-KO macrophage cells under TL compared with N/NL, despite significantly lower transcript levels (Figures 3B and 3C). G9a KD led to a significant reduction in protein expression for most m$^6$A regulators with minimal difference at the RNA level (Figures 3B and 3C). Taken together, these data suggested that G9a regulates/promotes expression, m$^6$A methyltransferase activity, and cytosolic localization of METTL3 in ET macrophages by a combination of translational and post-translational mechanisms.

Further, we investigated exactly how ET-activated G9a interacts with and regulates METTL3-mediated translation in the protein-specific control of chronic inflammation. We co-transfected equal amounts of HA-tagged G9a and Flag-tagged METTL3 into LPS-responsive 293/TLR4-MD2-CD14 cells[43] under different inflammatory conditions (N, NL, or TL). As expected, using "forward" (anti-HA) and "reverse" (anti-Flag) immunoprecipitation (IP), we confirmed that enhanced interaction between G9a and METTL3 occurred specifically in T or TL (ET), and that their

**Figure 3. G9a regulates activity, expression, and methylation of METTL3 during ET.**

(A) Bar chart depicting the effect of G9a depletion on level of m$^6$A modified RNA in Raw264.7 and THP-1 cells under different inflammatory conditions (N, NL, T, TL). Mean ± SD of three independent experiments. (Top): Knocking down G9a (shRNA) in Raw 264.7 macrophage cells reduced the total mRNA m$^6$A level in endotoxin tolerance condition. *p < 0.05. (Bottom): Knocking out G9a or METTL3 in THP-1 monocyte cells reduced the total mRNA m$^6$A level in endotoxin tolerance condition. *p < 0.05, **p < 0.01

(B and C) Heatmaps showing RNA-Seq (B) and LFQ proteomics (C) results for various m$^6$A regulators in wild-type versus G9a KO or METTL3 KO THP-1 cells under different inflammatory conditions (N, NL, TL). Two biological replicates were performed per condition with their median shown. Boxplot at top shows distribution of m$^6$A regulator signature in each column and results of pairwise comparisons are shown as ns = non-significant, *p < 0.05, **p < 0.01, ***p < 0.001, ****p < 0.0001. (See also Table S2).

(D) Immunoblots confirming LPS/time-dependent interaction between G9a and METTL3; (Left): HA-G9a and Flag-METTL3 (1:1) were co-transfected in naive (N) 293/TLR4-MD2-CD14 cells and their interaction confirmed by both "forward" HA-G9a IP and "reverse" Flag-METTL3 IP; (middle): Co-transfecting Flag-METTL3 and HA-G9a (1:3) in 293/TLR4-MD2-CD14 cells followed by HA-G9a IP confirmed increased G9a-METTL3 interaction in T/TL. Cell responses to LPS stimulation were monitored by p65 phosphorylation; (right): Time-course dependent interaction between Flag-METTL3 and HA-G9a (1:3) in 293-TLR4/CD14/MD2 cells following 1 μg/mL LPS treatment for indicated time points.

(E) Mapping the interacting domains of G9a and METTL3; (top): G9a mutant lacking its catalytic domain (D4) did not interact with METTL3; (bottom): C-terminus deletion (Δ 201-580) mutant of METTL3 (M1) did not interact with G9a.

(F) Schematic showing position of LC-MS/MS identified methylated lysine (K) residues across METTL3 protein. Circle color indicates whether methylation at a site increased (red), decreased (blue), or was not detected (gray) following UNC0642 (1 μM) treatment. NLS = nuclear localization signal; ZNF = zinc finger domain.

(G) Bar chart depicting changes in METTL3 methylation following UNC0642 treatment. Flag-METTL3 and HA-G9a were transiently transfected into 293/TLR4-MD2-CD14 cells that were subjected to LPS stimulation (TL) 24 h after transfection, along with 1 μM UNC0642 or DMSO treatment, followed by Flag-METTL3 enrichment, trypsinization, and LC-MS/MS analysis for identification and quantification of protein methylation. The y axis shows ratio of UNC0642 treated samples relative to DMSO-treated controls, normalized by total METTL3. Mean ± SD of three independent experiments each performed in duplicate, with each individual site identification represented by a dot. **p < 0.01, ***p < 0.001, ****p < 0.0001 compared to DMSO-treated control.

See also Figure S3; Table S2.

Please cite this article in press as: Muneer et al., Non-canonical function of histone methyltransferase G9a in the translational regulation of chronic inflammation, Cell Chemical Biology (2023), https://doi.org/10.1016/j.chembiol.2023.09.012



CellPress

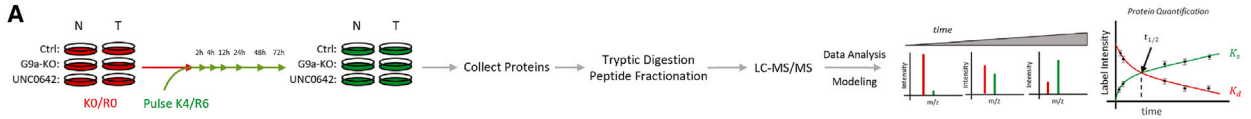


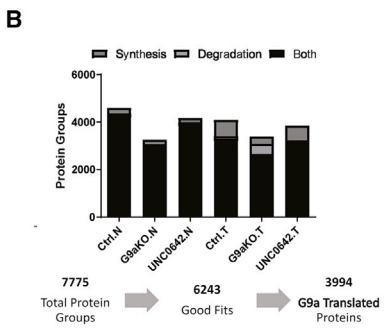


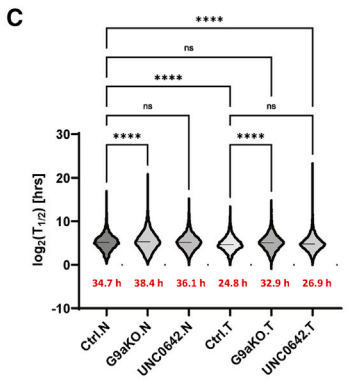


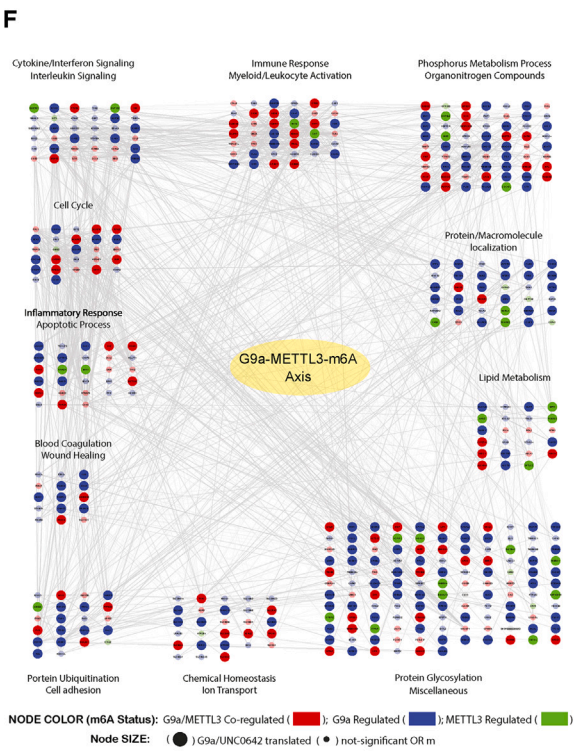


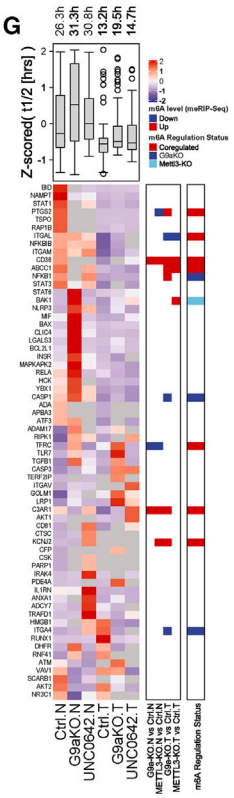


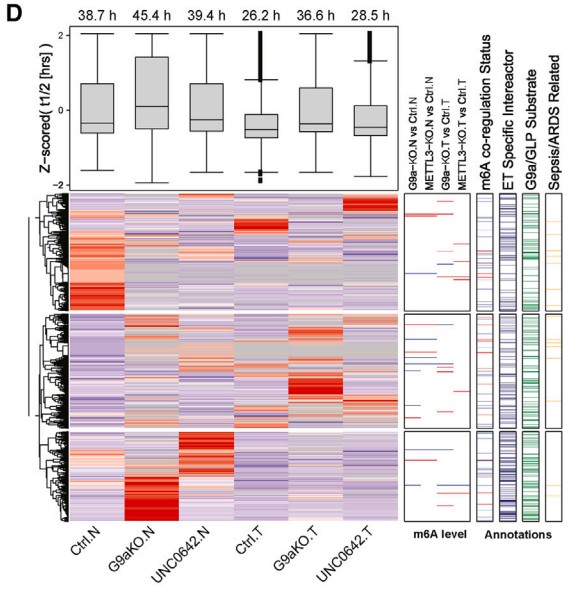


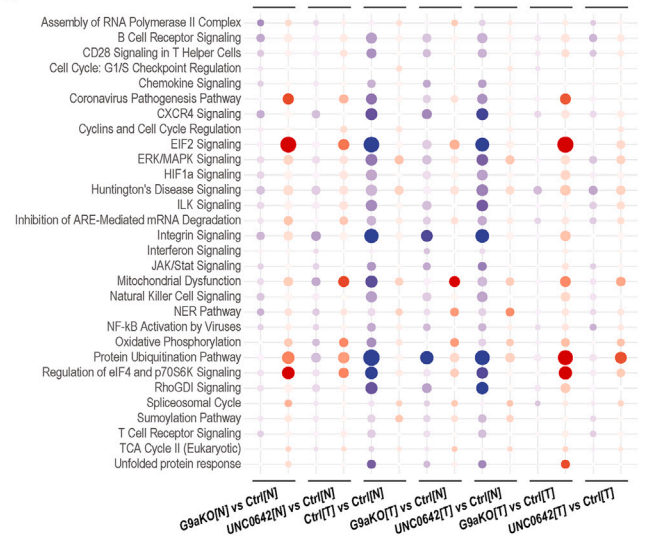


*FIGURE LEGEND:*

Median Z-scored (t1/2 [hrs])
-2 -1 0 1 2
m6A level (meRIP-Seq)
Down (FC < -1.5 ; Pval < 0.05 )
Up (FC > +1.5 ; Pval < 0.05)

*ROW ANNOTATIONS*
1. m6A co-regulation status (meRIP-Seq)
G9a/METTL3 Co-regulated [85]
G9a Regulated [170]
METTL3 Regulated [27]
2. G9a/GLP Interactor (ChaC)
ET Specific G9a/GLP Interactor [774]
3. G9a/GLP Substrates
G9a/GLP Substrate (Known/Putative) [760]
4. Sepsis/ARDS Related
Sepsis/ARDS Related Proteins [79]

*FIGURE LEGEND:*

Number of Genes in Pathway
0 10 20 30 40 50
Fisher's Exact Test [-log10(P)]
Faster Turnover
10 5 0 5 10
Slower Turnover

*(legend on next page)*

Please cite this article in press as: Muneer et al., Non-canonical function of histone methyltransferase G9a in the translational regulation of chronic inflammation, Cell Chemical Biology (2023), https://doi.org/10.1016/j.chembiol.2023.09.012



co-expression (input) and interaction increased with prolonged LPS stimulation that mimicked ET (Figure 3D). Next, using domain-truncated constructs, we showed that the catalytic SET domain of G9a interacts with the C-terminus region (aa 201–580) of METTL3 (Figure 3E). In coordination with the results from inhibitor competition ChaC analysis (Figure S1E), this domain mapping result suggested that G9a methylates METTL3 via G9a catalytic domain in ET. Phosphorylation,[44] SUMOylation,[45,46] and ubiquitination,[45] of METTL3 have been reported, suggesting the propensity of METTL3 to be post-translationally modified. However, literature on METTL3 methylation is lacking. Initially, we conducted methyltransferase activity analysis that showed that the G9a SET domain alone had negligible activity on purified METTL3 as opposed to nucleosome control *in vitro* (data not shown). This result suggested that, *in vivo*, G9a requires additional cofactors or acts as a scaffold to recruit other coenzyme(s) to facilitate METTL3 methylation. Therefore, to identify *in vivo* G9a methylation site(s) on METTL3, first, we carried out "forward" IP with anti-Flag (METTL3) antibody and "reverse" IP with anti-Kme1/me2/me3 antibody in the 293/TLR4-MD2-CD14 cells, which confirmed increased METTL3 methylation under LPS treated conditions (T and TL) compared with N/NL (Figures S3A and S3B). Then we used LC-MS/MS to sequence tryptic digests from the immunoprecipitated Flag-METTL3 and unambiguously identified six mono/di-methyl-lysines (K215, K281, K286, K296, K327, and K345), all within the C-terminus region of METTL3 (aa 201–580) that directly interacted with the catalytic SET domain of G9a (Figure 3F). Similarly, in line with immunoblotting results (Figure S3B), multiple METTL3 lysine residues (K215, K327) showed increased methylation in T or TL compared to N/NL conditions (Figure S3C).

Next, we identified differentially methylated lysine(s) on METTL3 following pharmacologic (UNC0642) inhibition of G9a during ET. UNC0642 is more than 20,000-fold selective/specific for G9a and GLP over 13 other methyltransferases ($IC_{50}$ > 50,000 nM) and more than 2,000-fold selective over PRC2-EZH2 ($IC_{50}$ > 5,000 nM).[29] Thus, any Kme site(s) that show UNC0642-suppressed abundance should be G9a regulated. Accordingly, we performed LFQ LC-MS/MS sequencing experiments on the METTL3 isolated from the 293/TLR4-MD2-CD14 cells with and without UNC0642 treatment under TL conditions. We unambiguously identified three methyl-lysine (Kme) residues, K286, R296, and K345, that showed UNC0642-reduced methylation, whereas K215me and K327me were not identified in high confidence in UNC0642-treated cells (Figure 3G), likely due to extremely low abundance of lysine methylation of nonhistone proteins. We also compared MS/MS-sequenced methylation regions of METTL3 with reported G9a-target motifs. Interestingly, K215 is in the S**RK**H motif that matches G9a-target sequence (A**RK**S) where R before K is critical for lysine methylation.[47,48] Moreover, K215 SUMOylation suppressed the $m^6A$ methyltransferase activity of METTL3,[45] and increased methylation at K215 in T/TL represents post-translational activation of METTL3 complex, thus explaining earlier observations (Figures 3A–3D, 1D, and S1G) of higher total $m^6A$ levels in T/TL despite lower levels of $m^6A$ regulator transcripts. Also, K215 is within the nuclear localization signal, potentially explaining the changes observed in METTL3 nuclear/cytosolic distribution following depletion or inhibition of G9a (Figure S1J). Altogether, multiple lines of evidence indicated that G9a-regulated METTL3 methylation is involved in ET translation.

## G9a accelerates global protein turnover in ET

ET-specific association of numerous translation regulators (Figures 1B and 1C), including known and putative substrates involved in rRNA/ribosome biogenesis (Figure S1E), together with polysome analysis results (Figure 1E) suggested that constitutively active G9a promotes global protein translation in ET macrophages, with partial contribution from the G9a-METTL3-$m^6A$ axis. To test this hypothesis and proteome-wide identification of "G9a-translated" proteins, we employed an amino acid coded tagging (AACT)[49] or SILAC pulse-labeling-based translatome[50] strategy to determine rates of synthesis, degradation, and overall turnover for individual proteins (Figure 4A and Methods S1). Briefly, cells grown in Lys0-Arg0 (K0/R0, "light", L) were pulse-labeled with Lys4-Arg6 (K4/R6, "medium", M) supplemented media. At 2h, 4h, 8h, 24h, 48h, and 72h after the medium switch, protein was extracted and subjected to tryptic digestion, fractionation, and LC-MS/MS. This experimental design yields (i) increasing signals from the K4R6-labeled protein molecules due to nascent protein synthesis and (ii) decreasing signals from K0R0-labeled proteins due to degradation or secretion of pre-existing protein molecules. Accordingly,

**Figure 4. G9a promotes global protein turnover, partly by the G9a-METTL3-$m^6A$ axis, and affects kinetics of numerous sepsis/ARDS-related proteins in ET macrophages**

(A) Overview of translatome strategy to determine protein half-lives (also see supplemental information).

(B) Bar chart depicting number of proteins in each condition for which turnover information was reliably calculated using label increase (syhtesis), label decrease (degradation), or both curves.

(C) Distribution of global protein turnover half-lives in different conditions are depicted using violin plots with median protein half-life for each condition [in hours] shown in red at bottom. $p < 0.0001$ (one-way ANOVA with Tukey's post hoc analysis, $F_{(5,23332)} = 63.01$). Asterisks indicate difference from control. ns = non-significant, ****$p < 0.0001$.

(D) Hierarchical clustering for median half-lives of G9a-translated proteins. Annotations on right depict G9a/GLP interactors (ChaC), nonhistone substrates of G9a/GLP and $m^6A$ modified genes (MeRIP-Seq) identified earlier in the study with frequency mentioned in the legend (in red). Boxplot at top shows distribution of protein half-lives in individual conditions with median of each condition depicted by the horizontal line inside the box and mentioned [in hrs] above each column.

(E) Pathway enrichment analysis for indicated comparisons. Size of the circle depicts number of proteins, and color depicts log transformed p value (also see Figure S5).

(F) Protein interaction network for G9a/METTL3 coregulated $m^6A$-target genes. G9a-translated proteins (~60%) and relevant pathways are shown.

(G) Heatmap showing that ET promotes turnover of inflammation/sepsis/ARDS-related proteins in macrophages, partly by the G9a-METTL3-$m^6A$ axis, whereas G9a loss/inhibition reverses this effect.

See also Figures S4 and S5; Table S3.

Please cite this article in press as: Muneer et al., Non-canonical function of histone methyltransferase G9a in the translational regulation of chronic inflammation, Cell Chemical Biology (2023), https://doi.org/10.1016/j.chembiol.2023.09.012





the inhibitor-induced rate changes in nascent protein synthesis or protein degradation were estimated by fitting the intensities of L or M labels at different time points in wild type, G9a KO, and UNC0642-treated macrophages under non-stimulated (N) or prolonged endotoxin stimulation (T) conditions (Figure 4A). The model assumed steady-state equilibrium conditions, in which the rate of increase was counterbalanced by the rate of decrease, leading to stable intracellular protein levels. Effects of amino acid recycling and differences in cell division rate between different conditions were also considered. Fit qualities were estimated using least-squared regression ($R^2$), root-mean-squared error (RMSE), and additional thresholds on fitted parameters to ensure good/meaningful estimates of protein turnover (Table S3A).

We obtained synthesis and/or degradation half-lives for 6,243 protein groups in the combined dataset (i.e., wild-type/Ctrl, G9a-KO, UNC0642-treated cells under N and T conditions). For 78–94% of fitted proteins, information was available for both AACT-label increase and decrease, which provided an internal duplicate measurement of protein turnover time for each sample in a steady-state system (Figure 4B; Table S3B). Half-life determination was reliable across labeling pairs (R = 0.99) and cell culture replicates (R = 0.29–0.99) as evidenced by Pearson correlation coefficients and covariance (Figures S4A and S4B). Under N and T conditions, whereas principal component analysis hinted at distinct proteostasis landscapes in macrophages, G9a knock-out or inhibition produced large effects on protein turnover compared with wild-type macrophages (Figure S4C). Consequently, we observed significant pairwise differences in global protein turnover time upon G9a inhibition as well as ET (Figure S4D). Estimated protein turnover times spanned four orders of magnitude (with some outliers), from minutes to thousands of hours. Accordingly, the rates of global translation or protein turnover were increased in ET as evidenced by shorter median half-lives in T (24.8–32.9 h) compared with N (34.7–38.4 h)-treated samples (Figure 4C). These ET-accelerated translation rates were reduced in G9a-KO or UNC0642-treated macrophages, specifically under T (32.9, 26.9h). Thus, in agreement with the polysome results that showed G9a-dependent protein synthesis (Figure 1C), this nonbiased translatome profiling indicated that G9a-interacting complexes accelerated global protein synthesis and degradation (i.e., global proteostasis) in ET macrophages.

## G9a-mediated translation unites multiple pathways associated with chronic inflammatory complications

Among the 6,243 proteins with AACT-quantified rates of turnover, 3,994 proteins showed G9a-dependent turnover based on pairwise comparisons of protein half-lives (Figure S4E). In line with global results, ET promoted turnover of G9a-translated proteins, whereas depletion or inhibition of G9a reversed this effect on global proteostasis landscape (Figure 4D). Overall, G9a promotes turnover of proteins involved in immune response, cell cycle, translation/proteostasis, cellular energetics, RNA biogenesis, and viral or coronavirus infection-related pathways (Figure 4E; Table S3C). Notably, 472 proteins with ET-characteristic turnover rates were encoded by G9a and/or METTL3-regulated $m^6A$ modified mRNAs, of which, 282 proteins (~60%) showed more than 2-fold difference in turnover rates in a G9a-dependent manner (Figure 4D; Table S3B). These $m^6A$-modified-mRNA encoded, G9a-translated proteins were primarily involved in immune response, inflammation, cell cycle, and cellular metabolism-related pathways (Figure 4F). Interestingly, we observed considerable variation in net protein turnover through individual pathways, which indicated that the global protein turnover trend did not completely capture the underlying complexity of G9a-regulated proteostasis in ET (Figure S5). Correspondingly, the G9a-METTL3-$m^6A$ axis accounted for only a subset of all G9a-translated proteins (i.e., 472 out of 3994), which suggested that via interactions with distinct translation regulators other than METTL3 (Figure 1B), G9a coordinates additional, as yet unknown, mechanisms to facilitate gene-specific translation to regulate chronic inflammation in ET macrophages. More importantly, our translatome strategy showed that G9a promoted turnover of 79 proteins associated with chronic inflammatory complications, such as sepsis and ARDS, in ET macrophages (Figure 4G). Genetic depletion or pharmacologic inhibition of G9a slowed turnover of sepsis or ARDS-related proteins, revealing a new mechanism of action in which G9a is an attractive target to suppress the translation of a range of immunopathogenic proteins.

Additionally, of the 3,994 G9a-translated proteins, 774 proteins were also identified by ChaC-MS as ET-phenotypic G9a interactors and 760 proteins were known or putative substrates[51,52] of G9a (Figure S4F; Table S3B). G9a-mediated methylation of the nonhistone substrate FOXO1 induces proteasomal degradation.[53] Therefore, our results not only support our identification of METTL3 as both a G9a interactor and a nonhistone substrate of G9a (Figure 3C), but the results also indicate that G9a may upregulate gene-specific turnover by interacting with or methylating select translation regulators. Overall, combined results from ChaC-MS, $m^6A$ RIP-Seq, and translatome analysis show that, via interacting or methylating various translation regulators, particularly METTL3, enzymatically active G9a upregulates the turnover of a battery of proteins to regulate chronic inflammation in ET and associated diseases.

## G9a-interacting translation regulators promote proteostasis of disease-related proteins

Bao et al. indicated the involvement of Ezh2 in the ARDS-associated pulmonary fibrosis.[54] Our translatome analysis revealed the G9a-dependent translation of PRC2 complex proteins in ET (see Table S3B), implicating G9a and Ezh2 in cooperatively regulating the translation of disease-related proteins. Because clinically validated inhibitors of Ezh2 are in antitumor clinical trials, we considered Ezh2 inhibitors for sepsis therapy and compared the proteomic effects of a G9a inhibitor (UNC0642) with an Ezh2 inhibitor (UNC1999).[55] We used various quantitative proteomic approaches,[24–26] i.e., LFQ or TMT-based quantitative methods, to quantify effect of enzymatic inhibition of G9a and Ezh2 on expression and secretion of sepsis- or ARDS-related proteins in ET macrophages (Figure S6A). Based on their overexpression in ET macrophages, we identified 43 and 34 proteins whose expression or secretion was suppressed by either or both inhibitors (Figures S6B and S6C) with immunoblotting

Please cite this article in press as: Muneer et al., Non-canonical function of histone methyltransferase G9a in the translational regulation of chronic inflammation, Cell Chemical Biology (2023), https://doi.org/10.1016/j.chembiol.2023.09.012



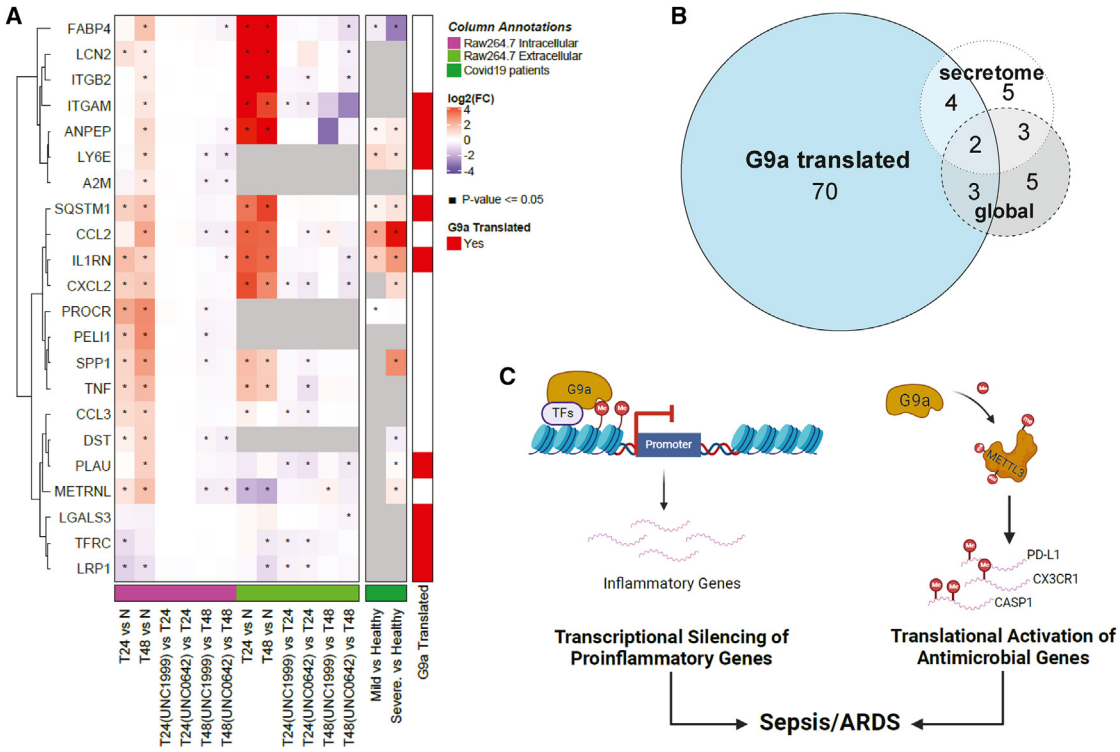


**Figure 5. Inhibition of G9a interactome enzymatic activity suppresses sepsis/ARDS related proteins**

(A) Heatmap showing decrease in expression and secretion of select sepsis/ARDS-related proteins in LPS tolerant ("T") Raw264.7 macrophages compared with naive ("N") cells upon pharmacologic inhibition of G9a (UNC0642, 1 μM) and Ezh2 (UNC1999, 1 μM). Cells were harvested 24h and 48h post-treatment. Statistically significant comparisons are marked by a dot, and annotations on right depict expression in COVID19 patients along with G9a-dependent translation status of the proteins.

(B) Venn diagram shows that G9a downregulates expression, secretion, and/or turnover of numerous sepsis and ARDS-related proteins in ET macrophages.

(C) Aberrantly activated G9a in ET macrophage cells suppresses transcription of pro-inflammatory genes while upregulating translation of anti-microbial/anti-inflammatory genes, in a METTL3 methyltransferase activity-dependent ($m^6A$) manner, to promote hyperinflammation and associated pathologies including sepsis and ARDS.

See also Figure S6; Table S4.

results being consistent with our mass-spectrometric findings (Figure S6D). More importantly, 22 sepsis- or ARDS-related proteins that showed overexpression in ET (T) macrophages compared to naive (N) cells also showed reduced expression and/or secretion following inhibition of G9a and/or Ezh2, with translation of 9 of these proteins being controlled by G9a (Figure 5A; Table S4). Interestingly, sepsis and ARDS are leading complications associated with severe COVID-19[56,57] and several ET-dysregulated UNC0642/UNC1999-reversed proteins identified were aberrantly expressed in mild/severe COVID-19 patients, compared with healthy controls (Figure 5A). Altogether, combined with translatome results, G9a promotes proteostasis (e.g., expression, secretion, and turnover) of 92 sepsis- and ARDS-related proteins in ET macrophage (Figure 5B). Moreover, G9a and Ezh2 cooperatively regulate sepsis- or ARDS-characteristic inflammation, at least during the course of inhibitor treatment, primarily by altering protein turnover as opposed to changing protein expression and/or secretion. More importantly, G9a inhibition reduces turnover (see Figure 4G) as well as expression and secretion (see Figure 5A) of numerous sepsis/ARDS-related proteins, making it an attractive target for treatment of chronic inflammation related-pathologies.

## DISCUSSION

### G9a has a non-canonical function in gene-specific translational control of chronic inflammation

Transcriptional mechanisms chart the host inflammatory response to infection by expressing proteins that control of inflammation. Prior to this study, the best-understood function of G9a/GLP was suppression of transcription of select pro-inflammatory genes. This function did not explain how the expression of certain antimicrobial (anti-inflammatory) genes is upregulated in ET wherein G9a is enzymatically active. Here, we reveal a new biological concept that G9a, a well-understood epigenetic regulator, complexes with translation regulatory machinery to produce proteins that contribute to chronic inflammatory pathogenesis.

Our ChaC-MS analysis of ET macrophages revealed that constitutively active G9a may act as a global regulator of multiple pathways that involve translation regulators. As the first step to elucidate G9a translational mechanisms, we determined how G9a regulates METTL3-mediated translation.[18] Using multi-omics approaches, we showed that G9a and METTL3 co-upregulate expression of select $m^6A$-tagged mRNAs involved in the

Please cite this article in press as: Muneer et al., Non-canonical function of histone methyltransferase G9a in the translational regulation of chronic inflammation, Cell Chemical Biology (2023), https://doi.org/10.1016/j.chembiol.2023.09.012



host hyperinflammatory response and T cell dysfunction, two hallmarks of ET-related pathogenesis (Figures 1 and 2). We showed that G9a regulates expression, localization, and lysine methylation of METTL3 to promote its m$^6$A methyltransferase activity. The G9a SET domain interacts with the N-terminus (aa 201–580) region of METTL3, and UNC0642 treatment lowered METTL3 methylation *in vivo* (Figure 3). This ET-specific G9a-regulated methylation of METTL3 is consistent with ChaC identification of multiple translation regulators as known/putative substrates of G9a and GLP. More importantly, this result indicated the involvement of constitutively (enzymatically) active G9a in global translation mechanisms in ET.

Accordingly, using our quantitative translatome approach to specifically identify newly translated proteins or proteins undergoing degradation in a G9a activity-dependent manner, we confirmed that G9a activity mediates a widespread translation mechanism: G9a accelerates global turnover of proteins involved in regulatory pathways related to immunity, cell cycle, translation/proteostasis, cellular energetics, RNA biogenesis, and viral/coronavirus infection (Figure 4). Notably, our quantitative translatome approach precisely measured the real-time abundances of proteins with minimum contributions from gene transcription, a method superior to Ribo-seq that correlates actively translated mRNAs to protein products. The G9a-METTL3-m$^6$A axis accounted for only a subset of G9a-translated proteins which, coupled with ChaC-MS identification of numerous nonhistone substrates of G9a involved in translation/proteostasis, hints toward additional mechanisms by which aberrantly activated G9a controls protein turnover under chronic inflammatory conditions. In this regard, G9a-binding-quantitative ChaC-MS also identified regulators of ribosome biogenesis as G9a interactors in ET macrophages, including members of FBL/NOP56-associated pre-rRNA complex that directs 2′-*O*-methylation-dependent translation. Indeed, global and secretome proteomic studies of G9a/Ezh2 inhibitor effects further revealed that G9a promotes proteostasis (expression, secretion. and/or turnover) of numerous proteins related to sepsis or ARDS (Figure 5). Altogether, we discovered that G9a has a novel, non-canonical (non-epigenetic) function in translational control of chronic inflammation, partly through the G9a-METTL3-m$^6$A axis.

## Inhibition of G9a translational mechanism for effective intervention of chronic inflammatory diseases

We showed that G9a interacts with METTL3 to promote proliferation of inflammatory cytokine-producing macrophages (hyperinflammation), reduce proliferation of CD8$^+$ T cells, and impair T cell function (lymphopenia) by promoting overexpression of immune checkpoint proteins such as PD-L1 (*CD274*) and CD25 (*IL2RA*) (Figure 2), both proteins being hallmarks of ET-related complications such as sepsis, ARDS, and COVID-19. Importantly, absence of G9a and METTL3 reversed these effects and restored T cell function, which indicated that G9a and its interactome (EZH2) can be targeted to reverse systemic cytokine profiles in sepsis, ARDS, and COVID-19 by reducing proteostasis (expression, secretion, and/or turnover) of 92 hyperinflammation-related proteins (Figures 4, 5, and S6). As proteins are the actual executors of disease and regulation of protein synthesis occurs on a much faster timescale compared with gene transcription,[58] targeting a translational regulatory mechanism is a more specific and robust approach to therapeutic intervention. Bypassing *de novo* nuclear control (epigenetic) mechanisms, pharmaceutical inhibition of G9a can directly suppress translation of a spectrum of immunopathologic genes to disrupt the disease-driving proteome. Thus, unlike most anti-inflammatory and anti-viral therapies that target one protein/epitope at a time and are susceptible to escape mutations, targeting host pathogenesis-related mechanisms like G9a-activated gene-specific translation is a more effective approach to treat sepsis and ARDS.

## Limitations of the study

Findings in this study should be considered in light of the following limitations that could be addressed by additional research. First, we have an incomplete picture of the mechanism by which G9a regulates METTL3 methylation while the functional consequences of individual methyl-lysine residues remain elusive—although UNC0642 regulated methyl-lysine residues near the ZNF1/ZNF2 domains (Figure 3F), which may affect METTL3 RNA substrate recognition. We note that G9a regulated methylation of METTL3 affected METTL3-eIF3 interaction (data not shown); non-methylatable mutants of METTL3 weakened METTL3 interaction with eIF3 by approximately 30%, which requires further investigation. Owing to low abundance of nonhistone protein methylation (less than 5% of parental proteins), unambiguous detection of methylation-dependent binding changes in replicates are technically challenging. Therefore, we removed this G9a methylation-dependent mechanism from this paper. Second, despite identification of most m$^6$A regulators, we did not detect endogenous METTL3 by ChaC-MS (Figure 1B), however, we confirmed ET-specific G9a-METTL3 interaction by multiple approaches including immunoblotting (Figures 1D and S1G), co-overexpression/co-IP (Figure 3D), and domain mapping (Figure 3E). The reasons for this discrepancy could be: (1) UNC0965 and METTL3 share binding sites on G9a′s SET domain, (2) MS in ‘‘top_n’’ mode missed low-abundance proteins, and (3) METTL3 peptides had poor ionization and low signal-to-noise ratio in MS. Third, this study largely focused on G9a-KO cells lines, as G9a-KO was more potent in hindering protein turnover/translation, compared to UNC0642 treatment alone, as evidenced by polysome and translatome results (Figures 1E, 4C, and 4D). However, because of high specificity and potency of UNC0642 toward both G9a and GLP (IC50 < 2.5nM), our translatome approach precisely identified/profiled the proteome whose translation is coregulated by G9a and GLP. Therefore, further studies to dissect the exact role of GLP during G9a/GLP complex-mediated translation are needed. Fourth, G9a, Ezh2, and METTL3 were all induced in ET macrophages (Figures 1B and S1G). Interestingly, we showed that G9a depletion suppressed METTL3 methyltransferase activity and expression, and other investigators reported that G9a[59] and EZH2[60] transcripts themselves carry m$^6$A modification and are stabilized by FTO (a m$^6$A eraser) and METTL3 (a m$^6$A writer) expression, respectively. Thus, possible crosstalk between the G9a, EZH2, and METTL3 complexes needs further investigation. Finally, although we focused on the G9a-METTL3-m$^6$A axis in this study, our ChaC-MS and translatome results indicated that G9a and GLP interact with various methyltransferases and E3 ligases to control other aspects of protein homeostasis that deserve further investigation.

Please cite this article in press as: Muneer et al., Non-canonical function of histone methyltransferase G9a in the translational regulation of chronic inflammation, Cell Chemical Biology (2023), https://doi.org/10.1016/j.chembiol.2023.09.012



## SIGNIFICANCE

**Endotoxin-tolerant (ET) macrophage cells have similar molecular/immunopathological characteristics as chronic inflammation-associated complications including sepsis and ARDS. These extreme responses of host immune system to persistent infection involve (1) suppression of "tolerizeable" pro-inflammatory genes coupled with (2) upregulation of "non-tolerizeable" anti-microbial (anti-inflammatory) factors that, together, contribute to impaired adaptive immunity and susceptibility to secondary infection with an organ-damaging "cytokine storm". However, despite significant clinical interest in ET, a unifying molecular mechanism that accounts for these two effects remains elusive. Prior to this study, the best-understood function of G9a/GLP was to suppress the transcription of select pro-inflammatory genes, which failed to interpretate how the expression of certain anti-microbial/anti-inflammatory genes is upregulated in ET wherein G9a is enzymatically active. Here, for the first time, we revealed a pivotal role of G9a in ET pathogenesis through its (a) canonical function in transcriptional repression of "tolerizeable" pro-inflammatory genes, and its (b) non-canonical/non-epigenetic function in promoting translation of "non-tolerizeable" anti-microbial/anti-inflammatory factors. Mechanistically, G9a interacts with translation regulators including METTL3, an N6-methyladenosine ($m^6A$) RNA methyltransferase, and methylates/activates it to cooperatively upregulate the translation and/or expression of certain $m^6A$-modified mRNAs to promote proliferation of inflammatory cytokine-producing macrophage cells (hyperinflammation), reduce proliferation of $CD8^+$ T cells, and impair T cell function (lymphopenia); both major hallmarks of COVID-19. Interestingly, G9a-METTL3-$m^6A$ axis accounted for only a subset of G9a-translated proteins in ET, suggesting that via interactions with distinct translation regulators other than METTL3, G9a coordinates additional, as yet unknown, mechanisms to facilitate gene-specific translation. More importantly, inhibition of G9a-regulated translation was shown to reverse hyperinflammation & lymphopenia and to hinder proteostasis (i.e., expression, secretion, and/or turnover) of numerous inflammatory disease-related factors involved in sepsis, ARDS, and COVID-19. Altogether, our findings represent an attractive target for host-pathogenesis-dependent therapeutic intervention to treat ET-related chronic inflammatory diseases.**

## STAR★METHODS

Detailed methods are provided in the online version of this paper and include the following:



## SUPPLEMENTAL INFORMATION

Supplemental information can be found online at https://doi.org/10.1016/j.chembiol.2023.09.012.

## ACKNOWLEDGMENTS

This work was supported by grants NIH 1R41DK133051-01A1, R01 GM133107-01, NIH R21AG071229, and the UNC University Cancer Research Fund (to X.C.), R01GM122749, R01HD088626, and an endowed professorship from the Icahn School of Medicine at Mount Sinai (to J.J.), and R01GM102413 (to J.G.C). The AVANCE NEO 600 MHz NMR Spectrometer System was upgraded with funding from a National Institutes of Health SIG grant 1S10OD025132-01A1.

## AUTHOR CONTRIBUTIONS

X.C. conceived and designed the project and experiments, analyzed, and interpreted data, and wrote the manuscript. A.M., L. W., and L.X. performed ChaC-MS and translatome experiments, biological and cell biology assays, and wrote the report. A.M. developed the software for translatome analysis and performed network analysis of clinical data. L.X. and E. H. F. performed inhibitor treatment, sample preparation and processing for MS/MS experimental analysis, and analyzed data. F. Z., J. S., and H.S. performed RNA-seq, MeRIP-seq, and analyzed the data. B.W. and Y.Y.W analyzed T cell activation/proliferation. L. M. and J.G.C performed cell cycle data collection and analysis. E.M.L. and N.J.M performed polysome experiments, and analyzed data. Y.X., W. Y., and J.J. provided UNC0965, UNC0642, and UNC1999. K. J. and B. D. S. performed *in vitro* methyltransferase assays.

## DECLARATION OF INTERESTS

This invention of the mechanism of inhibitor action is protected by United States Provisional Patent Application filed by the University of North Carolina-Chapel Hill (UNC 21–0060).

Received: November 1, 2021
Revised: June 21, 2023
Accepted: September 20, 2023
Published: October 19, 2023

Please cite this article in press as: Muneer et al., Non-canonical function of histone methyltransferase G9a in the translational regulation of chronic inflammation, Cell Chemical Biology (2023), https://doi.org/10.1016/j.chembiol.2023.09.012



CellPress

## REFERENCES


1. Cross, D., Drury, R., Hill, J., and Pollard, A.J. (2019). Epigenetics in Sepsis: Understanding Its Role in Endothelial Dysfunction, Immunosuppression, and Potential Therapeutics. Front. Immunol. *10*, 1363. https://doi.org/10.3389/fimmu.2019.01363.
2. Ciarlo, E., Savva, A., and Roger, T. (2013). Epigenetics in sepsis: targeting histone deacetylases. Int. J. Antimicrob. Agents *42*, S8–S12. https://doi.org/10.1016/j.ijantimicag.2013.04.004.
3. Newman-Toker, D.E., Schaffer, A.C., Yu-Moe, C.W., Nassery, N., Saber Tehrani, A.S., Clemens, G.D., Wang, Z., Zhu, Y., Fanai, M., and Siegal, D. (2019). Serious misdiagnosis-related harms in malpractice claims: The "Big Three" - vascular events, infections, and cancers. Diagnosis (Berl) *6*, 227–240. https://doi.org/10.1515/dx-2019-0019.
4. Assinger, A., Schrottmaier, W.C., Salzmann, M., and Rayes, J. (2019). Platelets in Sepsis: An Update on Experimental Models and Clinical Data. Front. Immunol. *10*, 1687. https://doi.org/10.3389/fimmu.2019.01687.
5. Giamarellos-Bourboulis, E.J. (2010). What is the pathophysiology of the septic host upon admission? Int. J. Antimicrob. Agents *36*, S2–S5. https://doi.org/10.1016/j.ijantimicag.2010.11.003.
6. Liu, D., Cao, S., Zhou, Y., and Xiong, Y. (2019). Recent advances in endotoxin tolerance. J. Cell. Biochem. *120*, 56–70. https://doi.org/10.1002/jcb.27547.
7. López-Collazo, E., and del Fresno, C. (2013). Pathophysiology of endotoxin tolerance: mechanisms and clinical consequences. Crit. Care *17*, 242. https://doi.org/10.1186/cc13110.
8. Foster, S.L., Hargreaves, D.C., and Medzhitov, R. (2007). Gene-specific control of inflammation by TLR-induced chromatin modifications. Nature *447*, 972–978.
9. Mages, J., Dietrich, H., and Lang, R. (2007). A genome-wide analysis of LPS tolerance in macrophages. Immunobiology *212*, 723–737.
10. Carpenter, S., Ricci, E.P., Mercier, B.C., Moore, M.J., and Fitzgerald, K.A. (2014). Post-transcriptional regulation of gene expression in innate immunity. Nat. Rev. Immunol. *14*, 361–376.
11. Hao, S., and Baltimore, D. (2009). The stability of mRNA influences the temporal order of the induction of genes encoding inflammatory molecules. Nat. Immunol. *10*, 281–288.
12. Jiang, L., Wang, Y., Zhu, D., Xue, Z., and Mao, H. (2016). Alteration of histone H3 lysine 9 dimethylation in peripheral white blood cells of septic patients with trauma and cancer. Mol. Med. Rep. *14*, 5467–5474. https://doi.org/10.3892/mmr.2016.5958.
13. Liu, C., Yu, Y., Liu, F., Wei, X., Wrobel, J.A., Gunawardena, H.P., Zhou, L., Jin, J., and Chen, X. (2014). A chromatin activity-based chemoproteomic approach reveals a transcriptional repressome for gene-specific silencing. Nat. Commun. *5*, 5733. https://doi.org/10.1038/ncomms6733.
14. Konze, K.D., Pattenden, S.G., Liu, F., Barsyte Lovejoy, D., Li, F., Simon, J.M., Davis, I.J., Vedadi, M., and Jin, J. (2014). A chemical tool for in vitro and in vivo precipitation of lysine methyltransferase G9a. ChemMedChem *9*, 549–553.
15. Wrobel, J.A., Xie, L., Wang, L., Liu, C., Rashid, N., Gallagher, K.K., Xiong, Y., Konze, K.D., Jin, J., Gatza, M.L., and Chen, X. (2019). Multi-omic Dissection of Oncogenically Active Epiproteomes Identifies Drivers of Proliferative and Invasive Breast Tumors. iScience *17*, 359–378. https://doi.org/10.1016/j.isci.2019.07.001.
16. Malovannaya, A., Lanz, R.B., Jung, S.Y., Bulynko, Y., Le, N.T., Chan, D.W., Ding, C., Shi, Y., Yucer, N., Krenciute, G., et al. (2011). Analysis of the human endogenous coregulator complexome. Cell *145*, 787–799. https://doi.org/10.1016/j.cell.2011.05.006.
17. Huttlin, E.L., Ting, L., Bruckner, R.J., Gebreab, F., Gygi, M.P., Szpyt, J., Tam, S., Zarraga, G., Colby, G., Baltier, K., et al. (2015). The BioPlex Network: A Systematic Exploration of the Human Interactome. Cell *162*, 425–440. https://doi.org/10.1016/j.cell.2015.06.043.
18. Lin, S., Choe, J., Du, P., Triboulet, R., and Gregory, R.I. (2016). The m(6)A Methyltransferase METTL3 Promotes Translation in Human Cancer Cells. Mol. Cell *62*, 335–345. https://doi.org/10.1016/j.molcel.2016.03.021.
19. Zong, X., Zhao, J., Wang, H., Lu, Z., Wang, F., Du, H., and Wang, Y. (2019). Mettl3 Deficiency Sustains Long-Chain Fatty Acid Absorption through Suppressing Traf6-Dependent Inflammation Response. J. Immunol. *202*, 567–578. https://doi.org/10.4049/jimmunol.1801151.
20. Lu, N., Li, X., Yu, J., Li, Y., Wang, C., Zhang, L., Wang, T., and Zhong, X. (2018). Curcumin Attenuates Lipopolysaccharide-Induced Hepatic Lipid Metabolism Disorder by Modification of m(6) A RNA Methylation in Piglets. Lipids *53*, 53–63. https://doi.org/10.1002/lipd.12023.
21. Feng, Z., Li, Q., Meng, R., Yi, B., and Xu, Q. (2018). METTL3 regulates alternative splicing of MyD88 upon the lipopolysaccharide-induced inflammatory response in human dental pulp cells. J. Cell Mol. Med. *22*, 2558–2568. https://doi.org/10.1111/jcmm.13491.
22. Wang, L., Muneer, A., Xie, L., Zhang, F., Wu, B., Mei, L., Lenarcic, E.M., Feng, E.H., Song, J., Xiong, Y., et al. (2020). Novel gene-specific translation mechanism of dysregulated, chronic inflammation reveals promising, multifaceted COVID-19 therapeutics. Preprint of bioRxiv. 2020.11.14.382416. https://doi.org/10.1101/2020.11.14.382416.
23. Hayano, T., Yanagida, M., Yamauchi, Y., Shinkawa, T., Isobe, T., and Takahashi, N. (2003). Proteomic analysis of human Nop56p-associated pre-ribosomal ribonucleoprotein complexes: possible link between Nop56p and the nucleolar protein treacle responsible for Treacher Collins syndrome. J. Biol. Chem. *278*, 34309–34319.
24. Ankney, J.A., Muneer, A., and Chen, X. (2018). Relative and Absolute Quantitation in Mass Spectrometry-Based Proteomics. Annu. Rev. Anal. Chem. *11*, 49–77. https://doi.org/10.1146/annurev-anchem-061516-045357.
25. Wang, L., Wrobel, J.A., Xie, L., Li, D., Zurlo, G., Shen, H., Yang, P., Wang, Z., Peng, Y., Gunawardena, H.P., et al. (2018). Novel RNA-Affinity Proteogenomics Dissects Tumor Heterogeneity for Revealing Personalized Markers in Precision Prognosis of Cancer. Cell Chem. Biol. *25*, 619–633.e5. https://doi.org/10.1016/j.chembiol.2018.01.016.
26. Feltcher, M.E., Gunawardena, H.P., Zulauf, K.E., Malik, S., Griffin, J.E., Sassetti, C.M., Chen, X., and Braunstein, M. (2015). Label-free Quantitative Proteomics Reveals a Role for the Mycobacterium tuberculosis SecA2 Pathway in Exporting Solute Binding Proteins and Mce Transporters to the Cell Wall. Mol. Cell. Proteomics *14*, 1501–1516. https://doi.org/10.1074/mcp.M114.044685.
27. Pachot, A., Cazalis, M.A., Venet, F., Turrel, F., Faudot, C., Voirin, N., Diasparra, J., Bourgoin, N., Poitevin, F., Mougin, B., et al. (2008). Decreased expression of the fractalkine receptor CX3CR1 on circulating monocytes as new feature of sepsis-induced immunosuppression. J. Immunol. *180*, 6421–6429. https://doi.org/10.4049/jimmunol.180.9.6421.
28. Avendaño-Ortiz, J., Maroun-Eid, C., Martín-Quirós, A., Toledano, V., Cubillos-Zapata, C., Gómez-Campelo, P., Varela-Serrano, A., Casas-Martin, J., Llanos-González, E., Alvarez, E., et al. (2018). PD-L1 Overexpression During Endotoxin Tolerance Impairs the Adaptive Immune Response in Septic Patients via HIF1alpha. J. Infect. Dis. *217*, 393–404. https://doi.org/10.1093/infdis/jix279.
29. Liu, F., Barsyte-Lovejoy, D., Li, F., Xiong, Y., Korboukh, V., Huang, X.-P., Allali-Hassani, A., Janzen, W.P., Roth, B.L., Frye, S.V., et al. (2013). Discovery of an in vivo chemical probe of the lysine methyltransferases G9a and GLP. J. Med. Chem. *56*, 8931–8942.
30. Arend, K.C., Lenarcic, E.M., and Moorman, N.J. (2018). The 5' Untranslated Region of the Major Immediate Early mRNA Is Necessary for Efficient Human Cytomegalovirus Replication. J. Virol. *92*, e02128-17. https://doi.org/10.1128/JVI.02128-17.
31. Hamy, A.S., Bieche, I., Lehmann-Che, J., Scott, V., Bertheau, P., Guinebretière, J.M., Matthieu, M.C., Sigal-Zafrani, B., Tembo, O., Marty, M., et al. (2016). BIRC5 (survivin): a pejorative prognostic marker in stage II/III breast cancer with no response to neoadjuvant chemotherapy. Breast

Please cite this article in press as: Muneer et al., Non-canonical function of histone methyltransferase G9a in the translational regulation of chronic inflammation, Cell Chemical Biology (2023), https://doi.org/10.1016/j.chembiol.2023.09.012



Cancer Res. Treat. *159*, 499–511. https://doi.org/10.1007/s10549-016-3961-2.

32. Kidokoro, T., Tanikawa, C., Furukawa, Y., Katagiri, T., Nakamura, Y., and Matsuda, K. (2008). CDC20, a potential cancer therapeutic target, is negatively regulated by p53. Oncogene *27*, 1562–1571. https://doi.org/10.1038/sj.onc.1210799.
33. Wang, Z., Wan, L., Zhong, J., Inuzuka, H., Liu, P., Sarkar, F.H., and Wei, W. (2013). Cdc20: a potential novel therapeutic target for cancer treatment. Curr. Pharm. Des. *19*, 3210–3214.
34. Gordon, C.A., Gong, X., Ganesh, D., and Brooks, J.D. (2017). NUSAP1 promotes invasion and metastasis of prostate cancer. Oncotarget *8*, 29935–29950. https://doi.org/10.18632/oncotarget.15604.
35. Gill, R.M., Gabor, T.V., Couzens, A.L., and Scheid, M.P. (2013). The MYC-associated protein CDCA7 is phosphorylated by AKT to regulate MYC-dependent apoptosis and transformation. Mol. Cell Biol. *33*, 498–513. https://doi.org/10.1128/MCB.00276-12.
36. Hu, R., Wang, M.Q., Niu, W.B., Wang, Y.J., Liu, Y.Y., Liu, L.Y., Wang, M., Zhong, J., You, H.Y., Wu, X.H., et al. (2018). SKA3 promotes cell proliferation and migration in cervical cancer by activating the PI3K/Akt signaling pathway. Cancer Cell Int. *18*, 183. https://doi.org/10.1186/s12935-018-0670-4.
37. Mahadevappa, R., Neves, H., Yuen, S.M., Bai, Y., McCrudden, C.M., Yuen, H.F., Wen, Q., Zhang, S.D., and Kwok, H.F. (2017). The prognostic significance of Cdc6 and Cdt1 in breast cancer. Sci. Rep. *7*, 985. https://doi.org/10.1038/s41598-017-00998-9.
38. Kobayashi, H., Komatsu, S., Ichikawa, D., Kawaguchi, T., Hirajima, S., Miyamae, M., Okajima, W., Ohashi, T., Kosuga, T., Konishi, H., et al. (2015). Overexpression of denticleless E3 ubiquitin protein ligase homolog (DTL) is related to poor outcome in gastric carcinoma. Oncotarget *6*, 36615–36624. https://doi.org/10.18632/oncotarget.5620.
39. Musa, J., Aynaud, M.M., Mirabeau, O., Delattre, O., and Grünewald, T.G. (2017). MYBL2 (B-Myb): a central regulator of cell proliferation, cell survival and differentiation involved in tumorigenesis. Cell Death Dis. *8*, e2895. https://doi.org/10.1038/cddis.2017.244.
40. Liu, S., Zhuo, L., Wang, J., Zhang, Q., Li, Q., Li, G., Yan, L., Jin, T., Pan, T., Sui, X., et al. (2020). METTL3 plays multiple functions in biological processes. Am. J. Cancer Res. *10*, 1631–1646.
41. Vu, L.P., Pickering, B.F., Cheng, Y., Zaccara, S., Nguyen, D., Minuesa, G., Chou, T., Chow, A., Saletore, Y., MacKay, M., et al. (2017). The N(6)-methyladenosine (m(6)A)-forming enzyme METTL3 controls myeloid differentiation of normal hematopoietic and leukemia cells. Nat. Med. *23*, 1369–1376. https://doi.org/10.1038/nm.4416.
42. Erdoğan, Ö., Xie, L., Wang, L., Wu, B., Kong, Q., Wan, Y., and Chen, X. (2016). Proteomic dissection of LPS-inducible, PHF8-dependent secretome reveals novel roles of PHF8 in TLR4-induced acute inflammation and T cell proliferation. Sci. Rep. *6*, 24833. https://doi.org/10.1038/srep24833.
43. Wang, T., Chuang, T.H., Ronni, T., Gu, S., Du, Y.C., Cai, H., Sun, H.Q., Yin, H.L., and Chen, X. (2006). Flightless I homolog negatively modulates the TLR pathway. J. Immunol. *176*, 1355–1362.
44. Schöller, E., Weichmann, F., Treiber, T., Ringle, S., Treiber, N., Flatley, A., Feederle, R., Bruckmann, A., and Meister, G. (2018). Interactions, localization, and phosphorylation of the m6A generating METTL3–METTL14–WTAP complex. Rna *24*, 499–512.
45. Du, Y., Hou, G., Zhang, H., Dou, J., He, J., Guo, Y., Li, L., Chen, R., Wang, Y., Deng, R., et al. (2018). SUMOylation of the m6A-RNA methyltransferase METTL3 modulates its function. Nucleic Acids Res. *46*, 5195–5208. https://doi.org/10.1093/nar/gky156.
46. Xu, H., Wang, H., Zhao, W., Fu, S., Li, Y., Ni, W., Xin, Y., Li, W., Yang, C., Bai, Y., et al. (2020). SUMO1 modification of methyltransferase-like 3 promotes tumor progression via regulating Snail mRNA homeostasis in hepatocellular carcinoma. Theranostics *10*, 5671–5686.
47. Rathert, P., Dhayalan, A., Murakami, M., Zhang, X., Tamas, R., Jurkowska, R., Komatsu, Y., Shinkai, Y., Cheng, X., and Jeltsch, A. (2008). Protein lysine methyltransferase G9a acts on non-histone targets. Nat. Chem. Biol. *4*, 344–346. https://doi.org/10.1038/nchembio.88.
48. Tsusaka, T., Kikuchi, M., Shimazu, T., Suzuki, T., Sohtome, Y., Akakabe, M., Sodeoka, M., Dohmae, N., Umehara, T., and Shinkai, Y. (2018). Trimethylation of ATF7IP by G9a/GLP recruits the chromodomain protein MPP8. Epigenet. Chromatin *11*, 56.
49. Zhu, H., Pan, S., Gu, S., Bradbury, E.M., and Chen, X. (2002). Amino acid residue specific stable isotope labeling for quantitative proteomics. Rapid Commun. Mass Spectrom. *16*, 2115–2123. https://doi.org/10.1002/rcm.831.
50. Schwanhäusser, B., Gossen, M., Dittmar, G., and Selbach, M. (2009). Global analysis of cellular protein translation by pulsed SILAC. Proteomics *9*, 205–209. https://doi.org/10.1002/pmic.200800275.
51. Islam, K., Bothwell, I., Chen, Y., Sengelaub, C., Wang, R., Deng, H., and Luo, M. (2012). Bioorthogonal profiling of protein methylation using azido derivative of S-adenosyl-L-methionine. J. Am. Chem. Soc. *134*, 5909–5915.
52. Islam, K., Chen, Y., Wu, H., Bothwell, I.R., Blum, G.J., Zeng, H., Dong, A., Zheng, W., Min, J., Deng, H., and Luo, M. (2013). Defining efficient enzyme–cofactor pairs for bioorthogonal profiling of protein methylation. Proc. Natl. Acad. Sci. USA. *110*, 16778–16783.
53. Chae, Y.-C., Kim, J.-Y., Park, J.W., Kim, K.-B., Oh, H., Lee, K.-H., and Seo, S.-B. (2019). FOXO1 degradation via G9a-mediated methylation promotes cell proliferation in colon cancer. Nucleic Acids Res. *47*, 1692–1705.
54. Bao, X., Liu, X., Liu, N., Zhuang, S., Yang, Q., Ren, H., Zhao, D., Bai, J., Zhou, X., and Tang, L. (2021). Inhibition of EZH2 prevents acute respiratory distress syndrome (ARDS)-associated pulmonary fibrosis by regulating the macrophage polarization phenotype. Respir. Res. *22*, 194. https://doi.org/10.1186/s12931-021-01785-x.
55. Konze, K.D., Ma, A., Li, F., Barsyte-Lovejoy, D., Parton, T., Macnevin, C.J., Liu, F., Gao, C., Huang, X.P., Kuznetsova, E., et al. (2013). An orally bioavailable chemical probe of the Lysine Methyltransferases EZH2 and EZH1. ACS Chem. Biol. *8*, 1324–1334. https://doi.org/10.1021/cb400133j.
56. Liu, D., Wang, Q., Zhang, H., Cui, L., Shen, F., Chen, Y., Sun, J., Gan, L., Sun, J., Wang, J., et al. (2020). Viral sepsis is a complication in patients with Novel Corona Virus Disease (COVID-19). Med. Drug Discov. *8*, 100057.
57. Swenson, K.E., and Swenson, E.R. (2021). Pathophysiology of acute respiratory distress syndrome and COVID-19 lung injury. Crit. Care Clin. *37*, 749–776.
58. Jiang, S.L., Mo, J.L., Peng, J., Lei, L., Yin, J.Y., Zhou, H.H., Liu, Z.Q., and Hong, W.X. (2021). Targeting translation regulators improves cancer therapy. Genomics *113*, 1247–1256. https://doi.org/10.1016/j.ygeno.2020.11.011.
59. Li, Y., Guo, X., Sun, L., Xiao, J., Su, S., Du, S., Li, Z., Wu, S., Liu, W., Mo, K., et al. (2020). N6-Methyladenosine Demethylase FTO Contributes to Neuropathic Pain by Stabilizing G9a Expression in Primary Sensory Neurons. Adv. Sci. *7*, 1902402.
60. Chen, J., Zhang, Y.-C., Huang, C., Shen, H., Sun, B., Cheng, X., Zhang, Y.-J., Yang, Y.-G., Shu, Q., Yang, Y., and Li, X. (2019). m6A regulates neurogenesis and neuronal development by modulating histone methyltransferase Ezh2. Dev. Reprod. Biol. *17*, 154–168.
61. Bian, C., Chen, Q., and Yu, X. (2015). Correction: The zinc finger proteins ZNF644 and WIZ regulate the G9a/GLP complex for gene repression. Elife *4*, e08168.
62. Lin, S., Choe, J., Du, P., Triboulet, R., and Gregory, R.I. (2016). The m6A methyltransferase METTL3 promotes translation in human cancer cells. Mol. Cell *62*, 335–345.
63. Bolger, A.M., Lohse, M., and Usadel, B. (2014). Trimmomatic: a flexible trimmer for Illumina sequence data. Bioinformatics *30*, 2114–2120.
64. Dobin, A., Davis, C.A., Schlesinger, F., Drenkow, J., Zaleski, C., Jha, S., Batut, P., Chaisson, M., and Gingeras, T.R. (2013). STAR: ultrafast universal RNA-seq aligner. Bioinformatics *29*, 15–21.

Please cite this article in press as: Muneer et al., Non-canonical function of histone methyltransferase G9a in the translational regulation of chronic inflammation, Cell Chemical Biology (2023), https://doi.org/10.1016/j.chembiol.2023.09.012



65. Li, H., Handsaker, B., Wysoker, A., Fennell, T., Ruan, J., Homer, N., Marth, G., Abecasis, G., and Durbin, R.; 1000 Genome Project Data Processing Subgroup (2009). The sequence alignment/map format and SAMtools. Bioinformatics *25*, 2078–2079.

66. Zecha, J., Satpathy, S., Kanashova, T., Avanessian, S.C., Kane, M.H., Clauser, K.R., Mertins, P., Carr, S.A., and Kuster, B. (2019). TMT labeling for the masses: a robust and cost-efficient, in-solution labeling approach. Mol. Cell. Proteomics *18*, 1468–1478.

67. Boisvert, F.-M., Ahmad, Y., Gierliński, M., Charrière, F., Lamont, D., Scott, M., Barton, G., and Lamond, A.I. (2012). A quantitative spatial proteomics analysis of proteome turnover in human cells. Mol. Cell. Proteomics *11*. M111.011429.

68. Welle, K.A., Zhang, T., Hryhorenko, J.R., Shen, S., Qu, J., and Ghaemmaghami, S. (2016). Time-resolved analysis of proteome dynamics by tandem mass tags and stable isotope labeling in cell culture (TMT-SILAC) hyperplexing. Mol. Cell. Proteomics *15*, 3551–3563.

69. Jovanovic, M., Rooney, M.S., Mertins, P., Przybylski, D., Chevrier, N., Satija, R., Rodriguez, E.H., Fields, A.P., Schwartz, S., Raychowdhury, R., et al. (2015). Dynamic profiling of the protein life cycle in response to pathogens. Science *347*, 1259038.

70. Ly, T., Endo, A., Brenes, A., Gierlinski, M., Afzal, V., Pawellek, A., and Lamond, A.I. (2018). Proteome-wide analysis of protein abundance and turnover remodelling during oncogenic transformation of human breast epithelial cells. Wellcome Open Res. *3*, 51.

71. Weng, Y.-L., Wang, X., An, R., Cassin, J., Vissers, C., Liu, Y., Liu, Y., Xu, T., Wang, X., Wong, S.Z.H., et al. (2018). Epitranscriptomic m6A regulation of axon regeneration in the adult mammalian nervous system. Neuron *97*, 313–325.e6.

72. Picelli, S., Faridani, O.R., Björklund, A.K., Winberg, G., Sagasser, S., and Sandberg, R. (2014). Full-length RNA-seq from single cells using Smart-seq2. Nat. Protoc. *9*, 171–181.

Please cite this article in press as: Muneer et al., Non-canonical function of histone methyltransferase G9a in the translational regulation of chronic inflammation, Cell Chemical Biology (2023), https://doi.org/10.1016/j.chembiol.2023.09.012



## STAR★METHODS

### KEY RESOURCES TABLE

| REAGENT or RESOURCE | SOURCE | IDENTIFIER |
|---|---|---|
| Antibodies | | |
| G9a | Millipore | Catalog # 07-551; RRID: AB_310709 |
| H3K9me2 | Millipore | Catalog # 07-441; RRID: AB_310619 |
| EIF4E | Proteintech | Catalog # 11149-1-AP; RRID: AB_2097686 |
| EIF3B | Proteintech | Catalog # 10319-1-AP; RRID: AB_2096732 |
| HNRNPA2B1 | Proteintech | Catalog # 14813-1-AP; RRID: AB_2279638 |
| METTL3 | Proteintech | Catalog # 15073-1-AP; RRID: AB_2142033 |
| PD-L1 | Proteintech | Catalog # 66248-1-Ig; RRID: AB_2918384 |
| YTHDF2 | Proteintech | Catalog # 24744-1-AP; RRID: AB_2687435 |
| CDC20 | Proteintech | Catalog # 10252-1-AP; RRID: AB_2229016 |
| CDCA7 | Proteintech | Catalog # 15249-1-AP; RRID: AB_2878119 |
| BIRC5 | Proteintech | Catalog # 10508-1-AP; RRID: AB_2064048 |
| TPX2 | Proteintech | Catalog # 11741-1-AP; RRID: AB_2208895 |
| TOP2A | Proteintech | Catalog # 24641-1-AP; RRID: AB_2879651 |
| NUSAP1 | Proteintech | Catalog # 12024-1-AP; RRID: AB_2157789 |
| SPP1 | Proteintech | Catalog # 22952-1-AP; RRID: AB_2783651 |
| SQSTM1 | Proteintech | Catalog # 18420-1-AP; RRID: AB_10694431 |
| ACTIN | Proteintech | Catalog # 60008-1-Ig; RRID: AB_2289225 |
| p-p65(S536) | Cell Signaling | Catalog # 3033; RRID: AB_331284 |
| Brg1 (H-88) | Santa Cruz | Catalog # sc-10768x; RRID: AB_2255022 |
| Anti-HA (clone HA-7) | Sigma | Catalog # H9658; RRID: AB_260092 |
| anti-flag M2 (clone M2) | Sigma | Catalog # F1804; RRID: AB_262044 |
| Anti-rabbit IgG, HRP-linked Antibody | Cell Signaling | Catalog #7074V; RRID: AB_2099233 |
| Anti-mouse IgG, HRP-linked Antibody | Cell Signaling | Catalog #7076V; RRID: AB_330924 |
| $m^6A$ polyclonal antibody | Synaptic Systems | Catalog #202003; RRID: AB_2279214 |
| Bacterial and virus strains | | |
| DH5a electro-competent bacterial cells | Invitrogen | Catalog # 11319019 |
| One shot Stbl3 chemically competent cells | Invitrogen | Catalog # C737303 |
| Chemicals, peptides, and recombinant proteins | | |
| jetPRIME | Polyplus | Catalog #114-15 |
| BsmBI | NEB | Catalog #R0580S |
| Puromycin | Sigma | Catalog #P8833 |
| DMEM | Gibco | Catalog #11965092 |
| RPMI-1640 | Gibco | Catalog #11875119 |
| FBS | Gibco | Catalog #26140079 |
| penicillin, and streptomycin | Gibco | Catalog #15140122 |
| unlabeled-Lysine | Cambridge Isotope | Catalog # ULM-8766-PK |
| D4-Lysine | Cambridge Isotope | Catalog # DLM-2640-PK |
| $^{13}C6^{15}N2$-Lysine | Cambridge Isotope | Catalog # CNLM-291-H-PK |
| unlabeled-Arginine | Cambridge Isotope | Catalog # ULM-8347-PK |
| $^{13}C6$-Arginine | Cambridge Isotope | Catalog # CLM-2265-H-PK |
| $^{13}C6^{15}N4$-Arginine | Cambridge Isotope | Catalog # CNLM-539-H-PK |
| dialyzed fetal bovine serum | Thermo Fisher | Catalog #88440 |
| SILAC DMEM | Thermo Fisher | Catalog #88364 |
| protease inhibitor cocktail | Sigma | Catalog #P8340 |

(*Continued on next page*)

Please cite this article in press as: Muneer et al., Non-canonical function of histone methyltransferase G9a in the translational regulation of chronic inflammation, Cell Chemical Biology (2023), https://doi.org/10.1016/j.chembiol.2023.09.012





*Continued*

| REAGENT or RESOURCE | SOURCE | IDENTIFIER |
|---|---|---|
| PMSF | Acros Organics | Catalog #215740100 |
| Cycloheximide | Sigma | Catalog # 66-81-9 |
| Igepal CA630 | Sigma | Catalog #I3021 |
| BCA assay kit | Thermo Fisher | Catalog #23225 |
| neutravidin-agarose | Thermo Fisher | Catalog #29201 |
| Sequence grade Trypsin | Promega | Catalog #V511C |
| C18 (Octadecyl) | Empore 3M | Catalog #2215 |
| MS grade trifluoroacetic acid | Thermo-Fisher | Catalog #85183 |
| 0.1% formic acid | Thermo-Fisher | Catalog #LS118-212 |
| ACN and 0.1% formic acid | Thermo-Fisher | Catalog #LS120-1 |
| Chemiluminescent HRP antibody detection reagent | Denville Scientific | Catalog #E2400 |
| Ultrapure LPS, E. coli 0111:B4 | Invivogen | Catalog # tlrl-3pelps |
| UNC0965 | Konze et al.[14] | N/A |
| UNC0642 | Liu et al.[29] | N/A |
| UNC1999 | Konze et al.[55] | N/A |
| TMT 11-plex Isobaric Labeling Reagent Kit | Thermo Fisher | Catalog # A34808 |
| RNeasy kit | Qiagen | Catalog # 74104 |
| M-MLV reverse transcriptase | Promega | Catalog # M170B |
| SYBR Green Master Mix | Thermo Fisher | Catalog # 0221 |
| EdU | Santa Cruz | Catalog # sc-284628 |
| Paraformaldehyde | Electron Microscopy Sciences | Catalog # 1571s |
| AF647-azide | Life Technologies | Catalog # A10277 |
| DAPI | Life Technologies | Catalog # D1306 |
| Dynabeads Oligo $(dT)_{25}$ | Thermo Fisher | Catalog # 61006 |
| Dynabeads Protein A | Thermo Fisher | Catalog # 10001D |
| $N^6$-Methyladenosine | Sigma-Aldrich | Catalog # M2780 |
| RNase Inhibitor | NEB | Catalog # M0314S |
| RNA Clean & Concentrator-5 kit | Zymo | Catalog # R1015 |
| SMARTScribe reverse transcriptase | Takara | Catalog # 639536 |
| Advantage Polymerase Mix | Takara | Catalog # 639201 |
| AMPure XP beads | Fisher Scientific | Catalog # A63880 |
| EZ Tn5 Transposase | Lucigen | Catalog # TNP92110 |
| KAPA HiFi hotstart readymix | EMSCO/FISHER | Catalog # KK2601 |
| KAPA Library Quantification Kit | Fisher | Catalog # NC0078468 |
| **Critical commercial assays** | | |
| Cell Counting kit-8 | Dojindo | Catalog #CK04-05 |
| m6A RNA Methylation Assay Kit | Abcam | Catalog # ab185912 |
| **Deposited data** | | |
| MS proteomics data | This paper | PRIDE: PXD044382 |
| RNA-Seq and MeRIP-Seq data | This paper | GEO: GSE240674 |
| **Experimental models: Cell lines** | | |
| Human: 293/TLR4-MD2-CD14 | Invivogen | Catalog # 293-mtlr4md2cd14 |
| Mouse: RAW 264.7 | ATCC | Catalog # TIB-71; RRID: CVCL_0493 |
| Human: THP-1 | ATCC | Catalog # TIB-202; RRID: CVCL_0006 |
| Human: 293T | ATCC | Catalog # CRL-3216; RRID: CVCL_0063 |
| **Oligonucleotides** | | |
| RT-PCR BIRC5 for CCACCGCATCTCTACATTCAAG | This paper | N/A |
| RT-PCR BIRC5 rev CAAGTCTGGCTCGTTCTCAG | This paper | N/A |

(*Continued on next page*)

Please cite this article in press as: Muneer et al., Non-canonical function of histone methyltransferase G9a in the translational regulation of chronic inflammation, Cell Chemical Biology (2023), https://doi.org/10.1016/j.chembiol.2023.09.012



*Continued*

| REAGENT or RESOURCE | SOURCE | IDENTIFIER |
|---|---|---|
| RT-PCR CD274 for TCACTTGGTAATTCTGGGAGC | This paper | N/A |
| RT-PCR CD274 rev CTTTGAGTTTGTATCTTGGATGCC | This paper | N/A |
| RT-PCR RGS13 for GGTGGAGCAGAATTTCTAGGG | This paper | N/A |
| RT-PCR RGS13 rev ACATGTTTCAGTGGGTTCCTG | This paper | N/A |
| RT-PCR CX3CR1 for CAGATCCAGAGGTTCCCTTG | This paper | N/A |
| RT-PCR CX3CR1 rev ACAGGAACACAGTCCCAAAG | This paper | N/A |
| RT-PCR GAPDH for CATGTTCGTCATGGGGTGAACCA | This paper | N/A |
| RT-PCR GAPDH rev AGTGATGGCATGGACTGTGGTCAT | This paper | N/A |
| sgRNA mG9a for ATGGCGGAAAGACAGCCCGT | This paper | N/A |
| sgRNA mG9a rev ACGGGCTGTCTTTCCGCCAT | This paper | N/A |
| sgRNA hG9a for CAGGGTTTCTTCACTACGAG | This paper | N/A |
| sgRNA hG9a rev CTCGTAGTGAAGAAACCCTG | This paper | N/A |
| sgRNA mMettl3 for AGAAAAGAAAGGTCTTGGAG | This paper | N/A |
| sgRNA mMettl3 rev CTCCAAGACCTTTCTTTTCT | This paper | N/A |
| sgRNA hMETTL3 for ATTCTGTGACTATGGAACCA | This paper | N/A |
| sgRNA hMETTL3 rev TGGTTCCATAGTCACAGAAT | This paper | N/A |
| **Recombinant DNA** | | |
| pcDNA4/myc-his vector | Invitrogen | Catalog #V86320 |
| LentiCRISPR V2 | Addgene | Catalog #52961; RRID: Addgene_52961 |
| pMD2.G | Addgene | Catalog #12259; RRID: Addgene_12259 |
| psPAX2 | Addgene | Catalog #12260; RRID: Addgene_12260 |
| pHA-G9a | Liu et al.[13] | N/A |
| pFlag-G9a-SBP | Bian et al.[61] | N/A |
| pFlag-G9a(D1)-SBP | Bian et al.[61] | N/A |
| pFlag-G9a(D2)-SBP | Bian et al.[61] | N/A |
| pFlag-G9a(D3)-SBP | Bian et al.[61] | N/A |
| pFlag-G9a(D4)-SBP | Bian et al.[61] | N/A |
| pFlag-CMV2-METTL3 | Lin et al.[62] | N/A |
| pFlag-ms2-METTL3 | Lin et al.[62] | N/A |
| pFlag-ms2-METTL3-(1-350) | Lin et al.[62] | N/A |
| pFlag-ms2-METTL3-(351-580) | Lin et al.[62] | N/A |
| pFlag-ms2-METTL3-(1-200) | Lin et al.[61] | N/A |
| **Software and algorithms** | | |
| The R Project | The R Project | https://www.r-project.org/ |
| MATLAB (R2017b) | Mathworks | https://www.mathworks.com/products/matlab.html |
| Cytoscape version 3.8.0 | Cytoscape Consortium | https://cytoscape.org/ |
| FCS Express 7 | *De Novo* Software | https://denovosoftware.com/ |
| GraphPad Prism 9 | GraphPad | https://www.graphpad.com/scientific-software/prism/ |
| bcl2fastq2 v2.17.1.14 | Illumina | https://github.com/igorbarinov/bcl2fastq |
| Trimmomatic-0.32 software | Bolger et al.[63] | https://github.com/usadellab/Trimmomatic |
| STAR v.2.5.2a | Dobin et al.[64] | https://github.com/alexdobin/STAR |
| Samtools-1.1 software | Li et al.[65] | http://samtools.sourceforge.net/ |
| Integrative Genomics Viewer (IGV) | Broad Institute | https://software.broadinstitute.org/software/igv/ |
| UCSC Genome Browser | UCSC | https://genome.ucsc.edu/ |
| Maxquant version 1.6.10.43 | Maxquant | https://www.maxquant.org/maxquant/ |
| Perseus version 1.5.1.6 | Perseus | https://www.maxquant.org/perseus/ |

(*Continued on next page*)

Please cite this article in press as: Muneer et al., Non-canonical function of histone methyltransferase G9a in the translational regulation of chronic inflammation, Cell Chemical Biology (2023), https://doi.org/10.1016/j.chembiol.2023.09.012





*Continued*

| REAGENT or RESOURCE | SOURCE | IDENTIFIER |
|---|---|---|
| Ingenuity Pathway Analysis | Qiagen | https://digitalinsights.qiagen.com/products-overview/discovery-insights-portfolio/analysis-and-visualization/qiagen-ipa/ |
| DAVID bioinfomatics | DAVID bioinfomatics | http://david.abcc.ncifcrf.gov/ |
| STRING | STRING | http://string-db.org/ |
| Other | | |
| Ultra2D nanoLC system | Eksigent | N/A |
| Easy nanoLC 1000 | Thermo Fisher | N/A |
| Q-Exactive HFX Orbitrap mass spectrometer | Thermo Fisher | N/A |
| Attune NxT | Beckman Coulter | N/A |
| NextSeq 550 | Illumina | N/A |
| NanoLC trap column | SCIEX | Catalog #5016752 |
| Acclaim Pepmap C18 RP column | Thermo Fisher | Catalog #164261 |

## RESOURCE AVAILABILITY

### Lead contact

Further information and requests for resources and reagents should be directed to and will be fulfilled by the lead contact, Xian Chen (xianc@e-mail.unc.edu).

### Materials availability

This study did not generate new unique reagents.

### Data and code availability

- RNA-Seq and MeRIP-Seq datasets have been deposited at the GEO repository and are publicly available as of the date of publication. Mass spectrometry proteomics datasets have been deposited to the ProteomeXchange Consortium via the PRIDE partner repository and are publicly available as of the date of publication. Accession numbers are listed in the key resources table. All other data reported in this paper will be shared by the lead contact upon request.
- This paper does not report original code.
- Any additional information required to reanalyze the data reported in this paper is available from the lead contact upon request.

## EXPERIMENTAL MODEL AND STUDY PARTICIPANT DETAILS

### Bacterial strains

For plasmid propagation, DH5a and stbl3 electro-competent bacterial cells were used and cultured in LB medium (plus 100 mg/ml ampicillin for selection) at 37C with shaking.

### Cell lines and treatment

HEK293T (female), 293/TLR4-MD2-CD14 (female) and murine Raw264.7 (male) cells were maintained in DMEM medium (Gibco) while THP-1 (male) cells were grown in RPMI 1640 medium (Gibco). All media were supplemented with 10% fetal bovine serum (Gibco) and 100 U/ml penicillin and streptomycin. Cells were grown at 37°C in humidified air with 5% carbon dioxide. For ChaC pull-down experiments, Raw264.7 cells were either unstimulated ('Naive' or 'N') or subjected to a single LPS stimulation with 1 μg/ml ('Naive+LPS' or 'NL') for 15 minutes to induce acute inflammation or first primed with 100 ng/ml LPS to induce endotoxin tolerance or chronic inflammation for 24 h ('Tolerance' or 'T'), followed by a second LPS challenge at 1 μg/ml for 15 minutes ('Tolerance+LPS' or 'TL'). For the condition requiring G9a inhibitor treatment, 1 μM UNC0642 was added at the time of cell plating. For global protein profiling, Raw264.7 cells were first pretreated with 100 ng/ml LPS for 24h ('T'), then inhibitor UNC1999 (1 μM) or UNC0642 (1 μM) was added, and cells were collected 8h, 24h and 48h post treatment. For MeRIP-Seq, THP-1 cells were first incubated in the presence of 60 nM PMA overnight to differentiate into macrophages followed by 48 h resting in PMA-free medium. Like Raw264.7 cells, THP-1 cells were either left unstimulated ('N') or subjected to a single LPS stimulation at 1 μg/ml for 15 min ('NL'), or first primed with 100 ng/ml LPS to induce endotoxin tolerance for 24 h ('T'), followed by the second LPS challenge at 1 μg/ml for 15 min ('TL').

Please cite this article in press as: Muneer et al., Non-canonical function of histone methyltransferase G9a in the translational regulation of chronic inflammation, Cell Chemical Biology (2023), https://doi.org/10.1016/j.chembiol.2023.09.012



## METHOD DETAILS

### Chemicals and reagents

All chemicals were HPLC-grade unless specifically indicated. Cell culture media, other components, and fetal bovine serum were obtained from Gibco. Trypsin was purchased from Promega. LPS (Escherichia coli 0111:B4, ultrapure) was purchased from InvivoGen (USA, Invivogen, cat# tlrl-3pelps). HEK 293 stable TLR4-MD2-CD14 cell line was also purchased from InvivoGen. Raw264.7 and THP1 cells were purchased from ATCC (Manassas, VA). UNC0642 (G9a inhibitor) and UNC1999 (EZH2 inhibitor)[55] were synthesized in Dr. Jian Jin's lab. TMT 11-plex isobaric labeling reagent kit was purchased from Thermo Fisher (Cat. A34808). Antibodies against G9a (07-551) and H3K9me2 (07-441) were from Millipore. Proteintech was the source of antibodies against EIF4E (11149-1-AP), EIF3B (10319-1-AP), HNRNPA2B1 (14813-1-AP), METTL3 (15073-1-AP), YTHDF2(24744-1-AP), PD-L1 (66248-1-Ig), CDC20 (10252-1-AP), CDCA7 (15249-1-AP), BIRC5 (10508-1-AP), TPX2 (11741-1-AP), TOP2A (24641-1-AP), NUSAP1 (12024-1-AP), SPP1 (22952-1-AP), SQSTM1 (18420-1-AP), and ACTIN (60008-1-Ig). Antibody against p-p65(S536) (3033) was from Cell Signaling. Antibody against Brg1 (H-88) (sc-10768x) was from Santa Cruz. Anti-HA (clone HA-7) and anti-flag M2 (clone M2) antibodies were from Sigma. An m6A RNA methylation quantification kit was from Abcam (ab185912).

### Plasmids

Plasmid pHA-G9a was described.[13] pFlag-CMV2-METTL3, pFlag-ms2-METTL3 and truncated expression plasmids were kindly provided by Dr. Richard I. Gregory.[62] Full-length pFlag-G9a-SBP and truncated plasmids (D1-D4) were kindly provided by Dr. Xiaochun Yu.[61]

### UNC0965 pull-down and ChaC sample processing

Similar to our recent report,[15] 1 mg nuclear protein extracted from Raw 264.7 macrophage cells was incubated overnight at 4°C with 2 nmole UNC0965 pre-coupled to 50 μl neutravidin-agarose (Thermo Fisher), and washed three times with 1 ml lysis buffer to remove non-specific proteins. For on-beads sampling and processing, five additional washes with 50 mM Tris-HCl pH 8.0, 150 mM NaCl were used to remove residual detergent. On-beads tryptic digestion was performed with 125 μl buffer containing 2 M urea, 50 mM Tris-HCl pH 8.0, 1 mM DTT, 500 ng trypsin (Promega) for 30 min at room temperature on a mixer (Eppendorf). The tryptic digests were eluted twice with a 100 μl elution buffer containing 2 M urea, 50 mM Tris-HCl pH 8.0, 5 mM iodoacetamide. Combined eluates were acidified with trifluoroacetic acid at final concentration of 1% (TFA, mass spec grade, Thermo Fisher Cat#85183) and desalted with a C18 stage tip.

### Sample preparation for TMT based global proteomic profiling

Cell pellets were resuspended in 8 M urea, 50 mM Tris-HCl pH 8.0, reduced with dithiothreitol (5 mM final) for 30 min at room temperature, and alkylated with iodoacetamide (15 mM final) for 45 min in the dark at ambient temperature. Samples were diluted 4-fold with 25 mM Tris-HCl pH 8.0, 1 mM $CaCl_2$ and digested with trypsin at 1:100 (w/w, trypsin:protein) ratio overnight at room temperature. Peptides were desalted on homemade C18 stage tips. Each peptide sample (100 μg) was labeled with 100 μg of TMT reagent following the optimal protocol.[66] The mixture of labeled peptides was desalted and fractionated into 12 fractions in 10 mM TMAB containing 5-40% acetonitrile.

### Polysome analysis

METTL3 KO, G9A KO, and control Raw 264.7 cells were cultured in 10 cm plates until 80% confluent at the time of harvest. Cells were treated with 100 μg/ml cycloheximide (CHX; Sigma Cat. #66-81-9) for 10 min at 37°C. Media were removed, and the cells were washed twice with 10 ml PBS containing 0.1 mg/ml CHX, scraped, pelleted by spinning for 10 min at 2200rpm at 4°C. The cells were resuspended with 1 ml lysis buffer (20 mM Tris-HCl, pH 7.4, 140 mM KCl, 5 mM $MgCl_2$, 1% Triton X-100, 10 mM DTT) containing 0.1 mg/ml CHX and swelled on ice for 10 min followed by passing through a 27-gauge needle 5 times to break the cell membrane. The lysate was centrifuged for 10 min, and the supernatant was carefully layered onto 10-50% sucrose gradients and centrifuged at 32,000 rpm (no brake) in a Beckman SW-40 rotor for 2 h at 4°C. Gradients were fractionated by monitoring absorbance 254 nm.

### Transfection and CRISPR knockout

293/TLR4-MD2-CD14 cells were seeded in 6-well plates for 24 h before transfection, and the constructs were transfected or co-transfected into cells using reagent jetPRIME (Polyplus). After 24 h, the cells were lysed directly in the plates by adding SDS-PAGE sample buffer, heating at 95°C for 5 min, and sonicating for 5 seconds to clear the lysate for immunoblotting.

For the CRISPR/Cas9 constructs, oligonucleotides for the sgRNA of human and mouse G9a and METTL3 (see key resources table), were annealed and cloned in BsmBI-digested lentiCRISPRv2 (Addgene plasmid #52961). The empty vector was used as a negative control. Viral production was performed with a standard protocol. In brief, 10 μg of plasmid, including target plasmid, pMD2.G (Addgene plasmid #12259) and psPAX2 (Addgene plasmid #12260) with a ratio of 10:5:9, was co-transfected into 293T cells with jetPRIME™. Virus-containing media were collected 48 hours after transfection. Cells at 60-80% confluency were incubated with the virus containing media for 24-48 hours, and then subjected to 1.0 μg/mL puromycin selection. After 4-7 days puromycin selection, the stably transfected cells were collected.

Please cite this article in press as: Muneer et al., Non-canonical function of histone methyltransferase G9a in the translational regulation of chronic inflammation, Cell Chemical Biology (2023), https://doi.org/10.1016/j.chembiol.2023.09.012





### RNA isolation and RT-PCR and m6A RNA methylation level

Total RNA was isolated using RNeasy kit (Qiagen, cat# 74104). First-strand cDNA was synthesized by M-MLV reverse transcriptase (Promega, cat# M170B) and diluted by a factor of 10 for quantitative PCR. Real-time PCR was performed using SYBR Green Master Mix (Thermo Fisher, cat# 0221). All measurements were normalized to GAPDH and represented as relative ratios. PCR primers for real-time PCR are summarized in key resources table. The m6A level of isolated RNA was measured by an m6A RNA methylation quantification kit (Abcam, cat# ab185912).

### Cell cycle and FACS analysis

For flow cytometry analyses of cell cycle, cells were incubated with 10 uM EdU (Santa Cruz, sc-284628) for 30 minutes before harvesting by trypsinization. Cells were washed with PBS and fixed with 4% paraformaldehyde (Electron Microscopy Sciences, 1571s) in PBS for 15 min at room temperature. Then 1% BSA-PBS was added and the cells were centrifuged. Fixed cells were permeabilized with 0.5% Triton X-100 in 1% BSA-PBS at room temperature for 15 min, then centrifuged. Cells were processed for EdU conjugation with 1 μM AF647-azide (Life Technologies, A10277) in 100 mM ascorbic Acid, 1 mM CuSO4, and PBS for 30 minutes at room temperature in the dark. Lastly, cells were washed and incubated in 1 μg/mL DAPI (Life Technologies, D1306) overnight at 4°C. Samples were run on an Attune NxT (Beckman Coulter) and analyzed with FCS Express 7 (*De Novo* Software).

### P14 CD8$^+$ T cell proliferation and activation

P14 CD8$^+$ T cell proliferation and activation assay was performed as described.[42] Briefly, CD8$^+$ T cells from a P14 transgenic mouse were first isolated with CD8a microbeads according to manufacturer's instruction. Isolated CD8$^+$ T cells were resuspended in 1 mL RPMI-1640 medium and either labeled with 1 mL of the 10 μM Carboxyfluorescein diacetate succinimidyl ester (CFSE) for 8 min at RT for proliferation assay or kept unlabeled for activation assay. METTL3 KO, G9a KO, and control Raw 264.7 cells were seeded in 6-well plates with indicated treatments followed by 50 μg/mL Mitomycin C treatment for 30 min at 37°C. Cells were washed twice with 1 mL PBS and then labeled with 0.4 mL of the 30 μg/mL GP33-41 peptide in PBS for 30 min at 37°C. One hundred thousand P14 T cells were co-cultured with 2 × $10^5$ control, METTL3 KO, and G9a KO cells in 96-well plates in RPMI medium containing 50 U/mL mIL-2. The proliferation and activation of CD8$^+$ T cells were assessed by flow-cytometry at day six.

### AACT pulse-labeling and measurement of protein turnover rates

G9a KO and control Raw 264.7 cells were cultured in AACT/SILAC DMEM medium supplemented with regular lysine and arginine (K0R0) and 10% dialyzed fetal bovine serum (Thermo Fisher), 1% penicillin, and streptomycin for five passages. Control, G9a KO, and UNC0642 treated (1 μM) cells were either untreated ('N') or treated with low dose (100 ng/ml) LPS to induce endotoxin tolerance ('T'). The cells were washed twice with PBS to remove light medium (K0R0), and then switched to heavy (K4R6) AACT DMEM medium containing stable isotope-enriched $D_4$-lysine and $^{13}C_6$-arginine to label newly synthesized proteins. The cells were harvested at 2h, 4h, 8h, 24h, 48h, and 72h, and lysed in 8 M urea containing 50 mM Tris-HCl pH 8.0. One hundred micrograms protein from each condition was digested with trypsin, desalted, and fractionated with C18 material (High pH) into eight fractions followed by LC-MS/MS analysis.

Mathematical equations used to model synthesis and degradation of proteins in cell-lines/conditions with different doubling times were inspired from models described previously[67–70] and are described in supplemental information (see Methods S1).

## QUANTIFICATION AND STATISTICAL ANALYSIS

### LC-MS/MS analysis

For ChaC pull-down samples, desalted peptide mixtures were dissolved in 30 μl 0.1% formic acid (Thermo Fisher). Peptide concentration was measured with Pierce™ Quantitative Colorimetric Peptide Assay (Thermo Fisher). In the Easy nanoLC- Q Exactive HFX setup, peptides were loaded on to a 15 cm C18 RP column (15 cm × 75 μm ID, C18, 2 μm, Acclaim Pepmap RSLC, Thermo Fisher) and eluted with a gradient of 2-30% buffer B at a constant flow rate of 300 nl/min for 30 min followed by 30% to 45% B in 5 min and 100% B for 10 min. The Q-Exactive HFX was also operated in the positive-ion mode but with a data-dependent top 20 method. Survey scans were acquired at a resolution of 60,000 at m/z 200. Up to the top 20 most abundant isotope patterns with charge $\geq$ 2 from the survey scan were selected with an isolation window of 1.5 m/z and fragmented by HCD with normalized collision energies of 27. The maximum ion injection time for the survey scan and the MS/MS scans was 100 ms, and the ion target values were set to 3e6 and 1e5, respectively. Selected sequenced ions were dynamically excluded for 30 seconds.

For global protein profiling, 0.5 μg of each fraction was analyzed on a Q-Exactive HF-X coupled with an Easy nanoLC 1200 (Thermo Fisher Scientific, San Jose, CA). Peptides were loaded on to a nanoEase MZ HSS T3 Column (100Å, 1.8 μm, 75 μm x 150 mm, Waters). Analytical separation of all peptides was achieved with 100-min gradient. A linear gradient of 5 to 10% buffer B over 5 min, 10% to 31% buffer B over 70 min and 31% to 75% buffer B over 15 minutes was executed at a 300 nl/min flow rate followed a ramp to 100%B in 1 min and 9-min wash with 100%B, where buffer A was aqueous 0.1% formic acid, and buffer B was 80% acetonitrile and 0.1% formic acid.

Peptides were separated with 45-min gradient, a linear gradient of 5 to 30% B over 29 min, 30 to 45% B over 6 min followed a ramp to 100%B in 1 min and 9-min wash with 100%B. LC-MS experiments were also performed in a data-dependent mode with full MS (externally calibrated to a mass accuracy of <5 ppm and a resolution of 120,000 for TMT-labeled samples or 60,000 for secretome

Please cite this article in press as: Muneer et al., Non-canonical function of histone methyltransferase G9a in the translational regulation of chronic inflammation, Cell Chemical Biology (2023), https://doi.org/10.1016/j.chembiol.2023.09.012



samples at *m/z* 200) followed by high energy collision-activated dissociation-MS/MS with a resolution of 45,000 for TMT-labeled global samples and 15,000 for secretome samples at *m/z* 200. High energy collision-activated dissociation-MS/MS was used to dissociate peptides at a normalized collision energy of 32 eV (for TMT-labeled sample) or 27 eV in the presence of nitrogen bath gas atoms. Dynamic exclusion was 45 or 20 seconds. Each fraction was subjected to three technical replicate LC-MS analyses. There were two biological replicates of samples and two technical replicates were executed for each sample.

### Proteomics data processing and analysis

Mass spectra were processed, and peptide identification was performed using the MaxQuant software version 1.6.10.43 (Max Planck Institute, Germany). All protein database searches were performed against the UniProt human protein sequence database (UP000005640). A false discovery rate (FDR) for both peptide-spectrum match (PSM) and protein assignment was set at 1%. Search parameters included up to two missed cleavages at Lys/Arg on the sequence, oxidation of methionine, and protein N-terminal acetylation as a dynamic modification. Carbamidomethylation of cysteine residues was considered as a static modification. Peptide identifications are reported by filtering of reverse and contaminant entries and assigning to their leading razor protein. The TMT reporter intensity found in MaxQuant was for quantitation. Data processing and statistical analysis were performed on Perseus (Version 1.6.0.7). Protein quantitation was performed using TMT reporter intensity found in MaxQuant and a one-sample t-test statistics on three technical replicates was used with a p-value of 5% to report statistically significant protein abundance fold-changes. Label-free quantification (LFQ) was for ChaC interactome and secretome data analysis.

### Analysis of functional category and networks

The biological processes and molecular functions of the G9a-interacting proteins were categorized by IPA (http://www.ingenuity.com/), DAVID (http://david.abcc.ncifcrf.gov/), and STRING (http://string-db.org/).

### m$^6$A RNA immunoprecipitation sequencing (MeRIP-Seq) and data analysis

m$^6$A-RIP-Seq was performed as described with slight modifications.[71] Messenger RNA from 10 ug total RNA extracted from Ctrl, METTL3 KO and G9a KO cell samples was purified with Dynabeads Oligo (dT)$_{25}$ (Thermo Fisher; 61006). Ten percent of 150 ng mRNA was used as Input mRNA, and the remainder was incubated with 3 ug anti-m$^6$A polyclonal antibody (Synaptic Systems; 202003) which was pre-conjugated to Dynabeads Protein A (Thermo Fisher; 10001D) in 500uL IP buffer (50 mM Tris, pH 7.4, 150 mM NaCl, 0.1% Igepal CA-630) for 2 hours at 4°C. After washing twice with IP-buffer and twice with High-Saltwash buffer (50 mM Tris pH 7.4, 500 mM NaCl, 0.1% Igepal CA-630) for 5 minutes each, the m6A mRNA was eluted with 100 uL IP-buffer containing 6.7 mM N$^6$-Methyladenosine (Sigma-Aldrich; M2780) and 40 U RNase Inhibitor (NEB, M0314S) and then recovered with RNA Clean and Concentrator-5 spin columns (Zymo; R1015).

The Input mRNA and m$^6$A-IPed mRNA were subjected to library generation using the SMART-seq protocol as described (Full-length RNA-seq from single cells using Smart-seq2).[72] For the synthesis of the first strand cDNA, the mRNA was mixed with 0.25 μL RNase inhibitor and 1 μL CDS primer (5'-AAGCAGTGGTATCAACGCAGAGTACT30VN-3') and heated to 70°C for 2 min. Then the mixture containing 0.5 μL of 100 mM DTT, 0.3 μL of 200 mM $MgCl_2$, 1 μL of 10 mM dNTPs, 0.25 μL RNase inhibitor, 1 μL of 10 μM TSO primer (5'-AAGCAGTGGTATCAACGCAGAGTACATrGrGrG-3'), 2 μL of 5X SMARTScribe RT buffer and 0.5 μL SMARTScribe reverse transcriptase (Takara, 639536) was added for performing reverse transcription. The cDNA was then amplified by Advantage Polymerase Mix (TAKARA, 639201) with IS primer (5'-AAGCAGTGGTATCAACGCAGAGT-3'). After purification with 0.8X AMPure XP beads (Fisher Scientific, A63880), the fragmentation of 100 pg cDNA was performed with EZ Tn5 Transposase (Lucigen, TNP92110). Fragments of cDNA were amplified by KAPA HiFi hotstart readymix (EMSCO/FISHER, KK2601) with the Nextera i7 primer and Nextera i5 primer. The DNA was purified with 0.8X AMPure XP beads and quantified by qPCR with KAPA Library Quantification Kit (Fisher, NC0078468). The DNA from different samples was pooled at equal molar amounts, and the final sequencing library was loaded at concentrations of 2.7 pM, and sequenced on a NextSeq 550 (Illumina) for single-read sequencing.

The raw sequencing data were demultiplexed with bcl2fastq2 v2.17.1.14 (Illumina) and the adapter was trimmed by Trimmomatic-0.32 software.[63] Then the Input and m6A-IP reads were mapped to human genome version hg38 by STAR v.2.5.2a,[64] and only uniquely mapping reads at the exon level for each gene were quantified and summarized to gene counts, which were further analyzed in R v.3.6.2 using DESeq2. After normalization, sorting, and indexing with Samtools-1.1 software,[65] the corresponding BAM files for each sample were loaded to UCSC genome browser to generate the peaks plots.